Redox Biology 71 (2024) 103100

Contents lists available at ScienceDirect

Redox Biology

journal homepage: www.elsevier.com/locate/redox

IL-13 facilitates ferroptotic death in asthmatic epithelial cells via SOCS1-mediated ubiquitinated degradation of SLC7A11

Manli Miao [a,b,c,f,1], Min Pan [a,b,c,1], Xu Chen [a,b,c,1], Jiapan Shen [a,b,c], Ling Zhang [a,b,c], Xiaoxia Feng [a,b,c], Mengting Chen [a,b,c], Guofeng Cui [a,b,c], Huaiyuan Zong [b], Wen Zhang [e], Shuang Chang [a,b,c], Fangzhou Xu [a,c], Zixi Wang [b], Dapeng Li [b,g], Weiwei Liu [b], Zhao Ding [b], Shengquan Zhang [b], Biao Chen [e,**], Xiaojun Zha [b,***], Xiaoyun Fan [a,c,d,*]

[a] Department of Geriatric Respiratory and Critical Care Medicine, The First Affiliated Hospital of Anhui Medical University, Hefei, China
[b] Department of Biochemistry & Molecular Biology, School of Basic Medicine, Anhui Medical University, Hefei, China
[c] Anhui Geriatric Institute, Hefei, China
[d] Key Laboratory of Respiratory Diseases Research and Medical Transformation of Anhui Province, Hefei, China
[e] Information Materials and Intelligent Sensing Laboratory of Anhui Province, Institutes of Physical Science and Information Technology, Anhui University, Hefei, China
[f] Department of Respiratory and Critical Care Medicine, Affiliated Hospital of Jining Medical University, Jining, China
[g] Department of Otolaryngology, Head and Neck Surgery, The Affiliated Bozhou Hospital of Anhui Medical University, Bozhou, China

ARTICLE INFO

Keywords:
Interleukin 13
Asthma
Ferroptosis
Suppressor of cytokine signaling 1
Solute carrier family 7 member 11
Airway epithelial cells

ABSTRACT

Th2-high asthma is characterized by elevated levels of type 2 cytokines, such as interleukin 13 (IL-13), and its prevalence has been increasing worldwide. Ferroptosis, a recently discovered type of programmed cell death, is involved in the pathological process of Th2-high asthma; however, the underlying mechanisms remain incompletely understood. In this study, we demonstrated that the serum level of malondialdehyde (MDA), an index of lipid peroxidation, positively correlated with IL-13 level and negatively correlated with the predicted forced expiratory volume in 1 s (FEV1%) in asthmatics. Furthermore, we showed that IL-13 facilitates ferroptosis by upregulating of suppressor of cytokine signaling 1 (SOCS1) through analyzing immortalized airway epithelial cells, human airway organoids, and the ovalbumin (OVA)-challenged asthma model. We identified that signal transducer and activator of transcription 6 (STAT6) promotes the transcription of SOCS1 upon IL-13 stimulation. Moreover, SOCS1, an E3 ubiquitin ligase, was found to bind to solute carrier family 7 member 11 (SLC7A11) and catalyze its ubiquitinated degradation, thereby promoting ferroptosis in airway epithelial cells. Last, we found that inhibiting SOCS1 can decrease ferroptosis in airway epithelial cells and alleviate airway hyperresponsiveness (AHR) in OVA-challenged wide-type mice, while SOCS1 overexpression exacerbated the above in OVA-challenged IL-13-knockout mice. Our findings reveal that the IL-13/STAT6/SOCS1/SLC7A11 pathway is a novel molecular mechanism for ferroptosis in Th2-high asthma, confirming that targeting ferroptosis in airway epithelial cells is a potential therapeutic strategy for Th2-high asthma.

1. Introduction

Asthma is one of the most common chronic non-communicable diseases and is estimated to be 300 million individuals globally [1], which characterized by damage to airway epithelial cells, airway hyperresponsiveness (AHR), airway inflammation, and mucus hypersecretion [2]. The airway epithelial cells represent the primary line of defense against foreign materials entering the airway. However, viruses, allergens, and toxic substances can damage airway epithelial cells and weaken airway defense, aggravating airway inflammation and AHR [3–7]. Two major endotypes of asthma have been described: the Th2-high and Th2-low [8]. Th2-high asthma is distinguished by high

* Corresponding author. Department of Geriatric Respiratory and Critical Care Medicine, the First Affiliated Hospital of Anhui Medical University, Hefei, China.
** Corresponding author.
*** Corresponding author.
E-mail addresses: cb0917@mail.ustc.edu.cn (B. Chen), zhaxiaojunpumc@gmail.com (X. Zha), 13956988552@126.com (X. Fan).
[1] Manli Miao, Min Pan, and Xu Chen contributed equally to this work.

https://doi.org/10.1016/j.redox.2024.103100
Received 31 January 2024; Accepted 19 February 2024
Available online 8 March 2024

levels of Th2-cytokines, such as interleukin (IL)-13, IL-5, and IL-4, in the serum and lung tissue [2]. IL-13 can damage airway epithelial cells and has a major influence on bronchial hyperreactivity [9–12]; however, the underlying mechanisms are not fully understood.

Ferroptosis is a newly identified form of regulated cell death characterized by the iron-dependent accumulation of lipid hydroperoxides and smaller mitochondria with condensed mitochondrial membrane densities [13]. Several signaling pathways are associated with ferroptosis, including the system xc^-/glutathione peroxidase 4 (GPX4) axis, iron metabolism pathway, lipid metabolism pathway, and amino-acid metabolism pathway [14]. Solute carrier family 7 member 11 (SLC7A11), the catalytic subunit of the cystine/glutamate antiporter system xc^-, has a well-established role in maintaining intracellular glutathione levels and protecting cells from ferroptosis [13,15]. Many studies have shown that ferroptosis participates in the occurrence and development of pulmonary diseases, including asthma [16–19]. However, these results are controversial. For example, Chen and colleagues showed that administering ferroptosis inhibitors (such as liproxstatin-1) can significantly decrease asthma inflammation and oxidative stress in murine asthma models [20]. Conversely, Wu et al. indicated that ferroptosis inducers (FINs), such as erastin and RAS-selective lethal 3 (RSL3), can inhibit inflammation in asthma by promoting eosinophil death [21]. Therefore, the specific role and underlying mechanism of ferroptosis in Th2-high asthma requires further investigation.

Here, we assessed clinical samples from asthmatic individuals, immortalized airway epithelial cells, human airway organoids (hAOs), and the ovalbumin (OVA)-challenged asthma model and uncovered a novel mechanism by which the IL-13/STAT6/SOCS1/SLC7A11 pathway enhances ferroptosis in airway epithelial cells and AHR in Th2-high asthma.

2. Materials and methods

2.1. Case selection and clinical samples obtain

A total of 56 asthmatic patients, diagnosed according to the Global Initiative for Asthma (GINA) guidelines (https://ginasthma.org/), and 25 healthy volunteers were enrolled in this study. All participants signed informed consent to participate in this research and underwent blood sampling. The levels of serum IL-13 and MDA for all patients and controls were measured. Basic information of all enrolled participants and clinical characteristics, including total serum IgE levels and FEV1%, of all asthmatic patients were collected. The Ethics Committee of the First Affiliated Hospital of Anhui Medical University approved this study (5101137).

2.2. Cell culture

As mentioned previously [22], human bronchial epithelial cells (BEAS-2B) and HEK-293T cells were obtained from the American Type Culture Collection (Manassas, VA, USA) and cultured in Dulbecco's modified Eagle's medium (DMEM, Hyclone, America). Human lung mucoepidermoid carcinoma cells (NCI–H292) were purchased from the Shanghai Institute of Life Sciences, Chinese Academy of Sciences (Shanghai, China) and cultured in Roswell Park Memorial Institute (RPMI)-1640 medium (Hyclone, America). All culture medium were complete medium supplemented with 10% fetal bovine serum (FBS, Technologies, Carlsbad, CA, USA), penicillin (100 μg/mL) and streptomycin (100 μg/mL) (Beyotime Biotechnology, Jiangsu, China). All of the cells were cultured under standard culture conditions (37 °C, 5% CO_2).

2.3. Organoid culture

Human embryonic stem cell (hESC) line H9 (WiCell Research Institute) was used to establish lung bud tip progenitor organoids (LPOs) as described previously [23]. Afterwards, to generate hAOs, LPOs were collected by gently pipetting and embedded in 60% Matrigel. After Matrigel solidified, LPOs in the gel were cultured with hAOs medium (Table S1): DMEM/F12 added with 50 nM dexamethasone, 100 μM 8-Br-cAMP, 100 μM IBMX, 10 ng/mL FGF7, 2% B-27 supplement, 0.25% Bovine Serum Albumin (BSA), and 0.1% ITS premix. The medium was changed every 3 days. A mechanical digestion process was used to transfer organoids every 3–7 days into new Matrigel droplets. Then, SOCS1 expression lentiviral vector or empty lentiviral vector was transfected into the organoids. The growth of the organoids was observed daily by microscopy.

2.4. Organoid viability

Acridine orange (Santa Cruz Biotechnology, CA, USA) and propidium iodide (Santa Cruz) (AO/PI) fluorescent dyes were used to detect organoid viability. After organoid digestion, 10 μL suspension and 10 μL AO/PI mixture were thoroughly mixed and incubated at 4 °C for 20 min, then the mixture was transferred to the cell counting plate. A cell fluorescence analyzer (Alit Biotech, Shanghai, China) was used to capture images of AO, green fluorescence, representing the live cells, of PI, red fluorescence, representing the dead cells. Then the organoid viability was calculated by the ratio of green and red fluorescence.

2.5. Reagents and antibodies

Recombinant human IL-13 was purchased from PeproTech (Cranbury, NJ, USA). RSL3, Erastin, AS1517499, MG-132, Homoharringtonine (HHT), and Leupeptin were obtained from Med Chem Express (MCE, NJ, USA). Dimethyl sulfoxide (DMSO) and OVA were purchased from Sigma Co., Ltd. (Louis, MO, USA). Western blot experiments were performed using the following antibodies: anti-SOCS1 (#ab280886), anti-SLC7A11 (#ab175186), anti-GPX4 (#ab125066), anti-STAT6 (#ab282107), anti-STAT6 (phospho Y641) (#ab263947), anti-p53 (#ab32389), and anti-NRF2 (#ab62352) from Abcam (Cambridge, MA, USA), anti-Ubiquitin (#3936), anti-K48-linkage Specific Polyubiquitin (#8146), anti-HA (#3724), anti-FLAG (#8146), and anti-Glyceraldehyde 3-phosphate dehydrogenase (GAPDH) (#5174) from Cell Signaling Technology (CST, Danvers, MA, USA), anti-MUC5AC (#abs126767) from Absin (Shanghai, China), anti-ACCTUB (#sc-23950) and anti-β-actin (#sc-47778) from Santa Cruz. Goat anti-rabbit IgG secondary antibody (#A0208) and goat anti-mouse IgG secondary antibody (#A0216) were obtained from Beyotime.

2.6. RNA interference

The STAT6-specific siRNAs were designed and synthesized by Shanghai GenePharma Company (Shanghai, China). The cells were transfected by using Lipofectamine RNAiMax (Thermo Fisher Scientific, USA) according to the manufacturer's instructions. The target sequences of the STAT6-siRNAs were derived from following sequences: siNC, 5′-UUCUCCGAACGUGUCACGUTT-3′; $siSTAT6^{-1}$, 5′-GCACCC UUGAGAGCAUAUATT-3′; $siSTAT6^{-2}$, 5′-CUGCACAGCUUGAUAGAAATT-3′; $siSTAT6^{-3}$, 5′-GGCUGAUCAUUGGCUUCAUTT-3′.

2.7. Lentivirus infection

The short hairpin RNAs (shRNA) were constructed and synthesized by GenePharma using the lentivirus vector LV2N (U6/Puro). The target sequences for knockdown (KD) of SOCS1 were as follows: shSC, 5′-TTCTCCGAACGTGTCACGT-3′; $shSOCS1^{-1}$, 5′- GACACGCACTTCCGCACATTC-3′; $shSOCS1^{-2}$, 5′-AGCAGCTTAACTGTATCTGGA-3′. The lentiviral vector LV6 (EF-1a/Puro) or LV11 (CMV/Neo) containing the full-length sequence of SOCS1 or SLC7A11 generated overexpression cell lines (GenePharma). Lentiviruses were transfected into cells according to the manufacturer's protocol. Stable cells were selected based on antibiotic resistance with puromycin (Solarbio, Beijing, China) or G-418

disulfate (Solarbio) of corresponding concentration. The efficiency of lentivirus infection was verified by Western blot and qRT-PCR.

2.8. Plasmids transfection

By using the full-length SOCS1 cDNA as templates, a series of plasmids constructing truncated SOCS1, including SOCS1-HA-N (amino acids 1–78), SOCS1-HA-SH2 (amino acids 79–174), SOCS1-HA-C (amino acids 175–211), SOCS1-HA-ΔN (depletion of amino acids 1–78), SOCS1-HA-ΔSH2 (depletion of amino acids 79–174), and SOCS1-HA-ΔC (depletion of amino acids 175–211), was cloned into pGMLV vector tagged by HA. The mutant plasmids of SLC7A11 were generated using PCR-based methods with specific primers and subsequently inserted into the pGMLV vector tagged by Flag. The above plasmids were designed and synthesized by Genomeditech (Shanghai, China) and transfected with lipofectamine 3000 reagents according to the manufacturer's protocol.

2.9. High-throughput RNA sequencing (RNA-Seq) analysis

Total RNA was extracted from cells using a TRIzol® Reagent Kit (Thermo Fisher) according to the manufacturer's instructions, and the concentration and purity of the RNA were checked using a NanoDrop instrument and the OD260/OD280 ratio. Subsequently, 1–2 μg of total RNA was used to construct the RNA-Seq libraries. We enriched mRNA and constructed libraries using the NEBNext® Poly(A) mRNA Magnetic Isolation Module (New England Biolabs, Beijing, China) and a KAPA Stranded RNA-Seq Library Prep kit (Illumina) according to the manufacturer's protocol. The sequencing library was examined by an Agilent 2100 Bioanalyzer and sequenced with an Illumina NovaSeq6000. Finally, genes with a fold change $\geq$1.5 and a P value $\leq$ 0.05 were defined as differentially expressed genes (DEGs). The RNA-seq was performed by Aksomics (Shanghai, China).

2.10. Bioinformatic analysis

RNA sequencing data of gene expression effects of IL-13 on primary human airway epithelial cells (GSE37697) were obtained from the Gene Expression Omnibus (GEO) dataset (http://www.ncbi.nlm.nih.gov/geo/). GEO2R was used to performed bioinformatic analysis. The ferroptosis-related genes were obtained from FerrDb (http://www.zhounan.org/ferrdb/current/).

2.11. Cell viability assay

Cell viability was detected by a Cell Counting Kit-8 kit (TargetMol, Shanghai, China) according to the manufacturer's protocols. Cells were cultured in 96-well plates (Corning, USA) and treated with IL-13 (100 ng/mL) for 72 h, followed by a range of concentrations of RSL3 for 24 h. Ten microliters of CCK8 assay reagent was added to each well and then incubated for 2 h in 5% CO_2 at 37 °C. Absorbance at a wavelength of 450 nm was measured using a microplate reader (ELX808, BioTek, Winooski, VT, USA).

2.12. Western blot analysis

Western blot analysis has been described previously [24]. Briefly, cells and tissues were denatured and electrophoresed by 10% SDS-polyacrylamide gel electrophoresis (SDS-PAGE) and transferred onto PVDF membranes (Millipore, Billerica, MA, USA). After blocking in 5% skimmed milk for 1 h, the membranes were incubated with primary antibodies at 4 °C overnight. The blots were then incubated with secondary antibodies at room temperature for 1 h and detected by chemiluminescence. The Western blot protein bands were analyzed using the Image J software.

2.13. Quantitative real-time polymerase chain reaction (qRT-PCR)

As described previously [25], total RNA from tissues or cells was extracted using Trizol Reagent (Life Technologies) and reverse transcribed into complementary DNA (cDNA) using a RevertAid™ First strand cDNA Synthesis Kit (Fermetas, Waltham, MA, USA). Real-time PCR was performed with SYBR Premix Ex Taq™ II (TaKaRa, Shiga, Japan), and the amount of RNA was analyzed using Bio-Rad CFX96 (Bio-Rad Laboratories, Hercules, CA). Other Genes expression levels were normalized to the signals of GAPDH expression. The primer sequences are listed in Table S2.

2.14. Immunofluorescence (IF) assay

BEAS-2B or NCI–H292 cells, after different treatments, were seeded onto coverslips and fixed with 4% paraformaldehyde (PFA) (MKCB4217, Sigma) for 30 min, then washed by PBS three times and permeabilized with 0.5% Triton X-100 (Beyotime) for 30 min. The cells were first incubated with anti-SOCS1 and anti-SLC7A11 antibodies at 4 °C overnight. After washing 3 times with PBS, the coverslips were incubated with a secondary antibody for 1 h at room temperature and sealed the slides with DAPI (Beyotime). Finally, the coverslips were observed under a fluorescence microscope (ZEISS, Oberkochen, Germany).

IF assay of hAOs has been described previously [23]. In brief, airway organoids were first covered with precooled cell recovery solution (1 mL each well), and then incubated on a horizontal shaker at 4 °C for 1 h. After washing for 3 times, organoids were fixed with 300 μL 4% PFA for 45 min at 4 °C, following permeabilized by 0.5% Tween 20 for 45 min. Then, the samples were blocked in 3% BSA in 0.1% Tween 20 for 60 min at room temperature and the primary antibodies were incubated overnight at 4 °C. The next day, after washing for 3 times, organoids were incubated with the secondary antibodies at room temperature for 90 min. Nuclear was stained with DAPI for 10 min at room temperature. Images were obtained using a Zeiss fluorescence microscope.

2.15. Enzyme-linked immunosorbent assay (ELISA) assay

The levels of IL-13 in serum samples from patients or bronchoalveolar lavage fluid (BALF) from asthma models were detected by IL-13 ELISA kits (R&D Systems, Minneapolis, MN, USA) according to the corresponding kit instructions.

2.16. Reporter constructs and dual-luciferase reporter assay

The *SOCS1* promoter was cloned into the *Bgl* III and *Kpn* I sites of the luciferase reporter plasmid pGL3-Basic (Promega, USA). The primer sequences used were as follows: forward, 5′-GAAGATCTTC GCTGCACCTCTCCCCAAAATG-3′; reverse, 5′-CGGGGTACCCCGGGC TGCCCTGGACTCCCCTC-3′. Three potential STAT6-binding sites on the promoter of the SOCS1 gene (site1, −674/−660, GTCAAGGAGCCTTTG; site2, −630/−616, GGGTTCCTCTGAAGC; site3, −600/−586, CGCTTCCCGGGAAGC) were mutated using Q5® Site-Directed Mutagenesis Kit (NEB, Ipswich, MA, USA). The primer sequences used were as follows: SOCS1-mut-R1, forward: 5′-CAGAACTGGGCCGGGGTGGAGGC-3′; reverse: 5′-GATCAACTGGGCGGGGCCGGG-3′; SOCS1-mutR2, forward: 5′-CTCTGAGCCTGTGGTCAGGCCGCCG-3′; reverse: 5′-TGAAC CCCTGGCGGCGCGGGC-3′; SOCS1-mut-R3, forward, 5′-AACA-GAGCCCGAGCCAAGACCAG-3′; reverse, 5′-AGAAGCGGCGGCCTGAC-CACAG-3′. For promoter activity analysis, the wild type (*WT*) or mutant SOCS1 promoter reporter vector was transfected into HEK-293T cells, and pRL-TK (20 ng) was used as an internal reference. The dual-luciferase reporter gene assay system (Promega) was used to detect luciferase activity.

2.17. Mass spectrometry (MS)

BEAS-2B cells, treated with IL-13 (100 ng/mL) for 72 h, were lysed in IP lysis. Then the cell lysate was centrifugated to collect the sample supernatant. Meanwhile, the anti-SLC7A11 or IgG antibodies were incubated with agarose beads at room temperature for 1 h. Subsequently, the sample supernatant was added into the agarose beads prepared above at 4 °C overnight. After washing, the samples were separated on 4–12% SDS-PAGE. The gel lanes were cut and harvested. Afterwards, the samples were subjected to Liquid Chromatography Mass Spectrometry by Bioprofile (Shanghai, China) to analyze proteins interacted with SLC7A11.

2.18. Molecular docking

The crystal structures of SH2-domain of SOCS1 and SLC7A11 were accessed from the RCSB PDB protein data bank (PDB, http://www.rcsb.org/pdb/). The obtained protein crystals were processed using the Protein Preparation Wizard module of Schrödinger software for a series of treatments, including pre-processing proteins, removing water molecules, and so on. The protein-protein docking module was used to dock the processed SH2-domain of SOCS1 with SLC7A11, set the number of ligand rotations to 70,000, and the maximum pose return to 30. The lower free energy of binding of the ligand to the receptor represented the higher binding stability.

2.19. Co-immunoprecipitation (Co-IP) assay

After corresponding treatments, cells were rinsed with cold PBS and lysed in cell lysis buffer for western and IP (Beyotime) on ice, and the total protein in the lysate served as the "Input" sample. Then, the anti-SOCS1, anti-SLC7A11, anti-HA, anti-FLAG, or IgG antibody were incubated with 20 μL protein G beads for 1 h at room temperature. The beads were incubated with cell lysate at 4 °C overnight, and washed with IP washing solution 3 times, then added 20 μL of 2 × SDS (Beyotime). Afterwards, the samples were detected by Western blot using antibodies against SOCS1, SLC7A11, HA, and FLAG.

2.20. Ubiquitination assay

Cells in a logarithmic growth period were plated in 10 cm dishes and cultured for 24 h in 5% CO_2 at 37 °C. Then, the cells were treated with 10 μM MG-132. After 8 h, these cells were washed with PBS and lysed for immunoprecipitation assay using anti-SLC7A11 antibody followed by Western blot assay using anti-Ub or anti-K48-linkage specific polyubiquitin antibody to detect SLC7A11 ubiquitination.

2.21. OVA-induced asthma mouse model and therapeutic interventions

The animal ethics committee of Anhui Medical University approved the animal experimental procedures and welfare (No. LLSC20210231) of this study. Specific pathogen-free (SPF) female C57/BL6 mice (5 weeks old) and three pairs of heterozygous mice *Il-13*$^{+/-}$ C57/BL6 were purchased from the GemPharmatech Co., Ltd (Nanjing, China) and housed in the Experimental Animal Center, Anhui Medical University (Hefei, China), given free access to food and water, and used after 1 week of quarantine and acclimatization. Homozygous C57/BL6/JGpt-Il13em69Cd2548/Gpt (*Il-13*$^{-/-}$) mice were obtained after mating with heterozygous mice and only female *Il-13*$^{-/-}$ mice were used in this study.

For subsequent studies, the *WT* C57/BL6 mice were randomly divided into the control group, the OVA group, the OVA + Ferrostatin-1 (Fer-1, MCE) group, the OVA + LvNC group, the OVA + LvSOCS1 group, the OVA + LvSOCS1 + Fer-1 group, the OVA + siNC group, and the OVA + siSOCS1 group (n = 5 mice per group). The *Il-13*$^{-/-}$ mice were randomly divided into four groups as follows: the control group, the OVA group, the OVA + LvNC group, and the OVA + LvSOCS1 group (n = 5 mice per group). Mice in the OVA group were sensitized by intraperitoneal (i.p.) injection with 0.5 mg/ml OVA and 5 mg/ml alum on day 0 and day 7. From day 14 to day 21, mice received only 1% OVA intranasally (i.n., qd) aerosolized in an airtight box for 30 min per day. Meanwhile, mice in the OVA + siNC group and the OVA + siSOCS1 group received additional interventions, intratracheal (i.t.) instillations of a nonspecific control siRNA or target SOCS1 siRNA every other day (qod), throughout the challenge period. The 5′-cholesterol and 2′-O-Methyl oligonucleotide modified SOCS1 siRNA and control siRNA were designed and synthesized by Genomeditech. The target sequences of the SOCS1-siRNAs were derived from following sequences: siNC: 5′-UUCUCCGAACGUGUCACGUdTdT-3′; siSOCS1: 5′-GUGACUACCUGAGUUCCUUtt-3′. Mice in the OVA + LvNC group and the OVA + LvSOCS1 group received additional interventions, intratracheal (i.t.) instillations of target lentivirus as described in the timeline. Additionally, during the challenge stage, the mice in the Fer-1 group were administrated with Fer-1 (5 mg/kg) by intraperitoneal injection 1 h before OVA challenge. The control group included mice challenged with saline alone on the same schedule. On day 22, the mice were euthanized to collect peripheral blood, the BALF, and lung tissue for further analysis, as described previously [22,26].

2.22. In vivo AHR and pulmonary function test

Mice were anesthetized and then received tracheotomy and intubation. Subsequently, the trachea of mice was connected to the animal airway resistance and pulmonary compliance system (EMMS, Hants, UK) to measure AHR. Airway resistance was measured during the inhalation of increasing concentrations (0, 3.125, 6.25, 12.5, 25, 50, and 100 mg/mL) of methacholine (MCh, Sigma) in living anesthetized mice.

2.23. Histological analysis and immunohistochemistry (IHC) staining

Airway organoids were wash with PBS for 5 min, then fixed with 4% PFA at room temperature for 10 min and washed with PBS. Then, 2% agarose melt in ddH_2O was added it into the plate. After solidification, the agarose was cut off any excess. Next, the samples were processed via a standard procedure for dehydration of the organization and embedded with paraffin wax. Paraffin was cut into 5 μm thicknesses. Finally, paraffin sections were stained using standard protocols for hematoxylin and eosin (H&E) staining reagents.

The lung tissue of mice was embedded and fixed in paraffin, and H&E or periodic acid-Schiff (PAS) staining was performed to observe the histological changes. The evaluation methods of bronchitis score and goblet cell proliferation of mice in each group were the same as those mentioned previously [26].

The left lung was fixed in 4% paraffin, sectioned, embedded in paraffin, and cut to 5 μm. Tissue sections were dewaxed, rehydrated, pretreated with 10 mM sodium citrate (Ebiogo, #B009), protected from

Table 1
Clinical features of the subjects.

	Control	Asthma	χ^2/t/Z	P value
Gender				
Male	10	23	0.008	0.928
Female	15	33		
Age (years)	39.44 ± 11.73	44.96 ± 15.45	−1.593	0.115
IL-13 (pg/mL)	75.28 ± 23.66	147.30 (64.67, 206.45)	−3.548	**<0.001**
MDA (μM)	0.89 ± 0.59	1.97 (0.57, 2.66)	−2.486	**0.013**
IgE (mIU/mL)[a]	NA	201.50 (47.00, 330.00)	–	–
FEV1%[b]	NA	81.30 (38.30, 97.93)	–	–

χ^2 Test, Z Test and *t*–Test. *IL-13* interleukin 13, *MDA* malondialdehyde, *IgE* the serum total IgE, *FEV1%* percentage of predicted forced expiratory volume in 1 s.
[a] Data available for 46 asthmatic patients;
[b] Data available for 44 asthmatic patients.

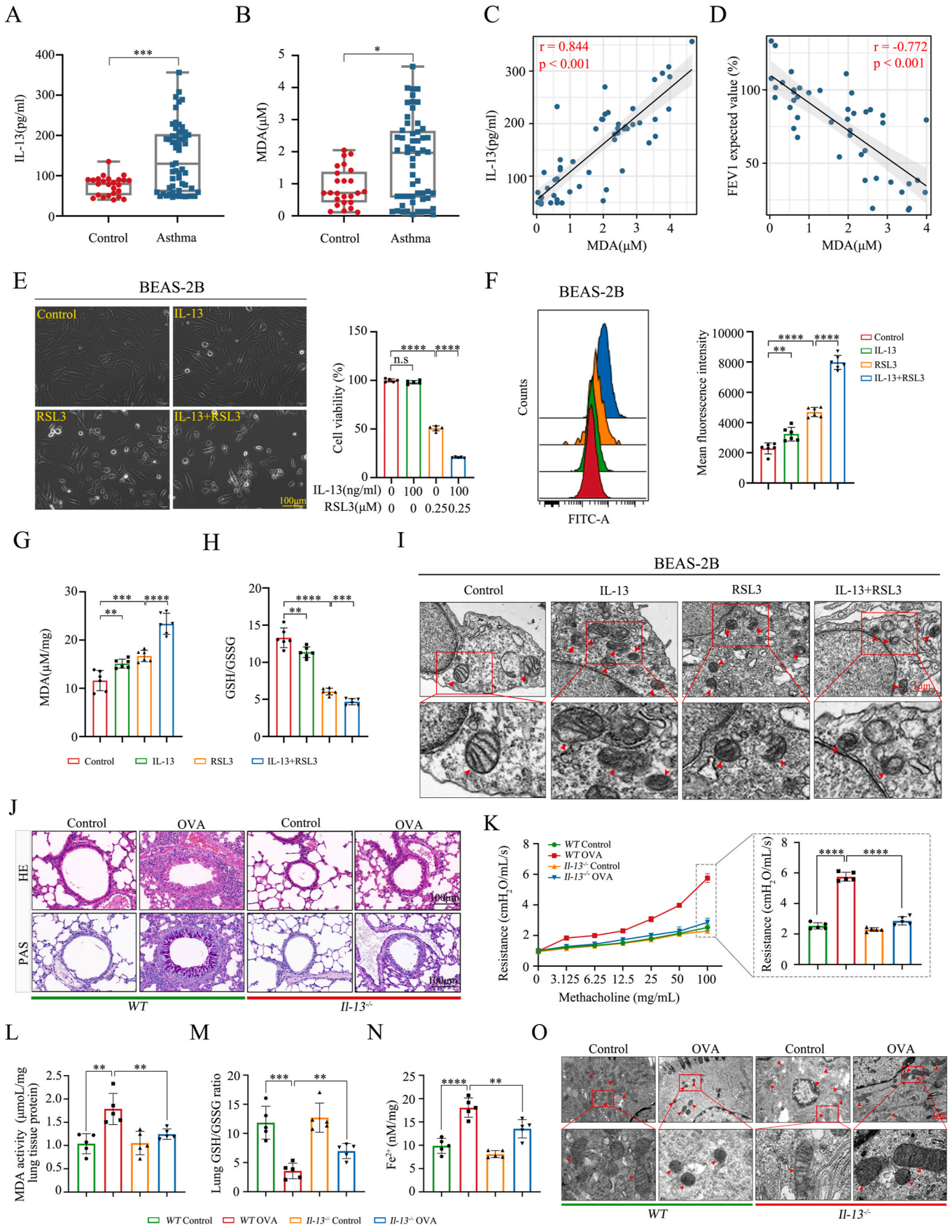

(caption on next page)

Fig. 1. IL-13 promotes FINs-induced ferroptosis in airway epithelial cells.
(A, B) IL-13 (A) and MDA (B) levels in serum from asthma patients (n = 56) and healthy controls (n = 25) were measured by ELISA and a MDA assay kit, respectively.
(C, D) The correlation between MDA levels and IL-13 levels (C) or FEV1 expected value% (D) of asthma patients was analyzed by the Pearson correlation statistic test.
(E) BEAS-2B cells were pretreated with or without IL-13 (100 ng/mL, 72 h), followed by RSL3 (0.25 μM, 24 h) treatment. The cell viability was detected by a CCK-8 kit (n = 5). Representative light microscope images (left panel). Scale bar: 100 μm. Statistical analysis chart (n = 5) (right panel).
(F) Lipid ROS in the indicated cells was measured by flow cytometry after C11-BODIY staining (n = 6).
(G, H) The intracellular MDA levels and GSH/GSSG ratio were measured by an MDA assay kit or a GSH and GSSG assay kit (n = 6).
(I) Representative TEM images of the indicated cells. Red arrows indicate mitochondria. Scale bar: 1 μm.
(J) Representative H&E staining (upper panels) and PAS staining (lower panels) images of lung tissues from *Il-13*$^{-/-}$ and *WT* mice. Scale bar: 100 μm.
(K) Airway resistance in response to increasing doses of Mch was measured 24 h after the final OVA exposure (n = 5).
(L, M) The MDA levels and GSH/GSSG ratio of lung tissues in the indicated mice were measured by an MDA assay kit or a GSH and GSSG assay kit (n = 5).
(N) The levels of Fe^{2+} in lung tissues in the indicated mice were measured by an iron assay kit (n = 5).
(O) Representative TEM images of the airway epithelial cell in the indicated mice. Red arrows indicate mitochondria. Scale bar: 1 μm.
*P < 0.05, **P < 0.01, ***P < 0.001, ****P < 0.0001 and n.s indicates no significance. (For interpretation of the references to colour in this figure legend, the reader is referred to the Web version of this article.)

endogenous peroxidase with 3% H_2O_2, and finally encapsulated within 5% BSA. Next, sections were incubated with primary antibodies, anti-SOCS1 (1:200, Abcam, #ab9870) and anti-SLC7A11 (1:200, Thermo Fisher, #XF3620408), at 4 °C overnight. After washing three times with PBS, the slides were incubated with a secondary antibody at 37 °C for 30 min. Subsequently, Diaminobenzidine (DAB, Ebiogo, #B011) was used as a chromogen, and the sections were counterstained with hematoxylin.

2.24. Transmission electron microscopy (TEM)

Cells were inoculated in 10 cm dishes (5×10^6 cells/dish), treated with the indicated drugs for the corresponding time, fixed with 4% PFA for 15 s, then collected, and further fixed with 2.5% glutaraldehyde. For airway organoids, the organoids were treated with the indicated drugs for the corresponding time, fixed with 4% PFA for 1 min, then collected, and further fixed with 2.5% glutaraldehyde. For tissue samples, the airway tissue was freshly isolated from the indicated mice and cut into small pieces (1 mm × 1 mm × 1 mm), then immediately fixed in 2.5% glutaraldehyde. The samples are dehydrated, permeabilized, embedded, sectioned, and cured to ultrathin sections (70 nm) with an ultramicrotome (Leica UC7, Leica). Subsequently, lead staining was performed, and images were obtained using a transmission electron microscope (JEM1400, Japan).

2.25. Lipid peroxidation(L-ROS) assay

The L-ROS level was analyzed by C11-BODIPY (581/591) (Thermo Fisher). Firstly, cells were seeded in 6-well plates. After indicated treatment, the cells were incubated in 2 μM C11-BODIPY (581/591) for 30 min at 37 °C in the dark, then measured using flow cytometry (CA, USA) through the green and red fluorescent signal channels of BODIPY™ 581/591C11 to detect changes in intracellular L-ROS according to the intensity of cell fluorescence.

2.26. MDA assay

The concentrations of MDA in cells and lung tissues were detected using the Lipid Peroxidation MDA Assay Kit (Beyotime) according to the product instructions. Briefly, for the measurement of MDA concentration in cells, the cells were inoculated in 6 cm dishes (about 2×10^6 cells/dish), treated with the indicated drugs for the corresponding time, then lysed by cell lysis solution, and the supernatant was collected after centrifugation, and the protein concentration of the cell samples was determined by the BCA kit (Beyotime). For tissues, 10 mg of tissues were homogenized after adding lysate, and the supernatant was collected after centrifugation. Samples were placed in a boiling water bath for 15 min and centrifuged at 1000 g for 10 min to retain supernatant. Afterwards, the supernatant was transferred to a 96-well plate, the absorbance value at 532 nm was detected using a microplate reader, and the MDA content in the sample was calculated.

2.27. Glutathione/glutathione disulfide (GSH/GSSG) ratio assay

The GSH levels and GSH/GSSG ratio in cells and lung tissues were detected using the GSH and GSSG Assay Kit (Beyotime) according to the product instructions. In brief, for cell samples, cells were cultured in 6 cm dishes, treated with the indicated drugs for the corresponding time, and then digested and collected. Subsequently, protein removal reagent M solution was added into cell suspension. The mixture was fully vortexed, and then centrifuged after two rapid freeze-thaws, and the supernatant was retained. For tissue samples, weighed tissue powder was added into protein removal reagent M solution. The mixture was fully vortexed, then centrifuged, and the supernatant was retained. The supernatant was fully mixed with corresponding reagents in the kit. Then the absorbance value at 412 nm was measured immediately by a microplate reader. Finally, the ratio of GSH to GSSG in the sample was calculated according to the standard curve and formula (GSH = Total Glutathione - GSSG × 2).

2.28. Iron assay

Ferrous iron levels in lung tissues of mice were measured by an iron assay kit (Abcam) according to the product instructions. Weighed tissue (10 mg for each assay) were homogenized in 4–10 vol of iron assay buffer followed by 16,000 g centrifugation for 10 min at 4 °C. Afterwards, incubation of iron buffer together with supernatant mixtures was conducted for 30 min. Samples were then cultured with iron probe for 1 h away from light. The absorbance values were measured at 593 nm. Finally, the levels of Fe^{2+} in the lung tissues were calculated according to the standard curve and formula.

2.29. Lactate dehydrogenase (LDH) assay

LDH levels in BALF of mice were detected by a LDH assay kit (Nanjing Jiancheng Bioengineering Institute, Nanjing, China) following the manufacturer's protocol. The BALF was centrifuged and then supernatant fully mixed with corresponding reagents was incubated. Finally, the absorbance value at 450 nm was measured, and then the LDH activity in BALF was calculated.

2.30. Statistical analysis

Data were analyzed and performed using GraphPad Prism (version 6) and IBM SPSS version 23.0 (IBM Corp., Armonk, NY, USA). Before making comparisons across values, the normality of distributions was tested using the Kolmogorov-Smirnov test. Differences in the distribution of individual features were analyzed using the χ^2 test for categorical variables and the Student's t-test or the Mann-Whitney *U* test for continuous variables. In addition, Pearson's correlation analysis was estimated to examine linear associations between the index. $P < 0.05$ was considered significant (*P < 0.05; **P < 0.01; ***P < 0.001; ****P

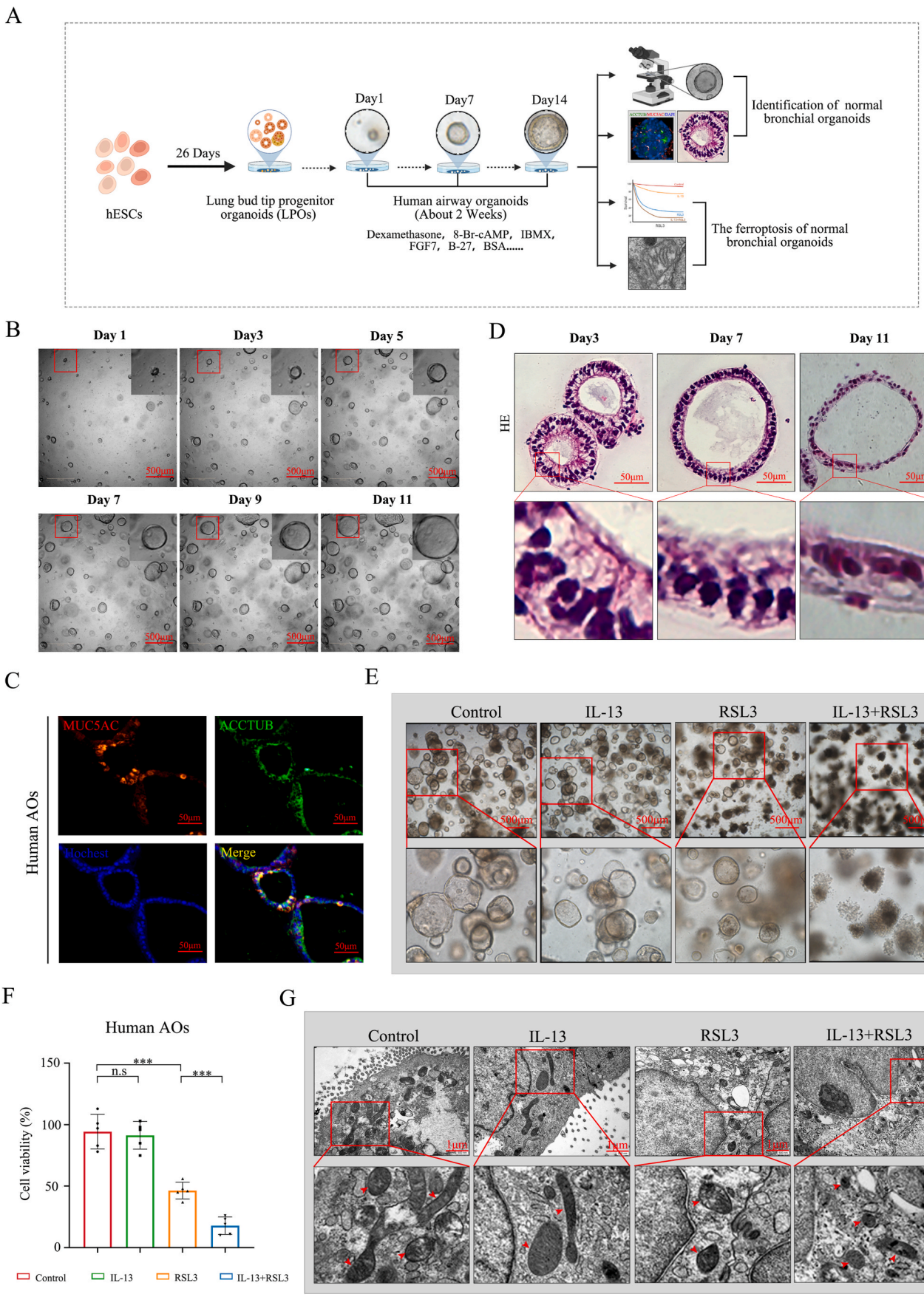

(caption on next page)

Fig. 2. IL-13 increases the sensitivity of hAOs to FINs.
(A) Workflow for the establishment and identification of hAOs.
(B) The hAOs were cultured in the original human AO medium for 14 d. Bright-field images of organoids at the indicated days are shown. Scale bar: 500 μm.
(C) Two lineages of airway epithelial cells (ACCUB^{+} ciliated cells and MUC5AC^{+} goblet cells) were identified in the hAOs via IF assay. Scale bar: 50 μm.
(D) Representative H&E staining images of hAOs at the indicated days. Scale bar: 50 μm.
(E–G) IL-13 (100 ng/mL, 72 h) pretreated hAOs were treated with or without RSL3 (10 μM) for 72 h. Morphological changes of hAOs (E). Scale bar: 500 μm. The viability of organoids was measured by a cell fluorescence analyzer (F) (n = 5). Representative TEM images (G). Red arrows indicate mitochondria. Scale bar: 1 μm. **P < 0.001 and n.s indicates no significance. (For interpretation of the references to colour in this figure legend, the reader is referred to the Web version of this article.)

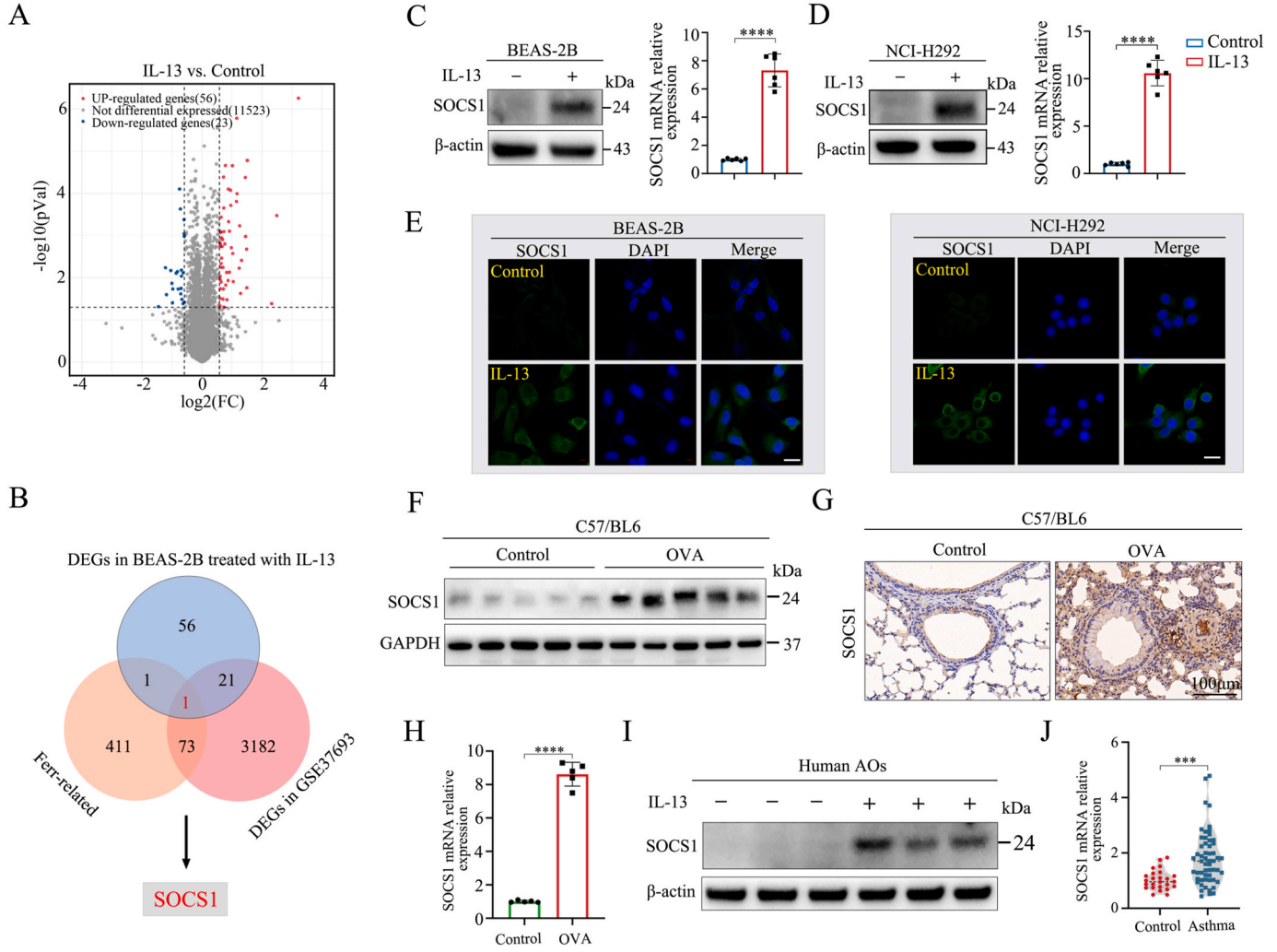

Fig. 3. IL-13 enhances SOCS1 expression.
(A) The RNA-seq volcano graph of DEGs between IL-13 (100 ng/mL, 72 h) and PBS (control) treated BEAS-2B cells. The red dots represent up-regulated DEGs, the blue dots represent down-regulated DEGs and the grey dots represent genes with no significant change.
(B) Venn diagram of the co-expressed DEG among the three datasets. Dataset 1 represents the DEGs between IL-13 (100 ng/mL, 72 h) and PBS-treated BEAS-2B cells. Dataset 2 represents DEGs of GSE37693. Dataset 3 represents ferroptosis-related genes.
(C–E) BEAS-2B and NCI–H292 cells were treated with IL-13 (100 ng/mL, 72 h) or PBS. The levels of SOCS1 were determined by Western blot (C left panel and D left panel), qRT-PCR (C right panel and D right panel), and IF staining (E) (n = 6). Scale bar: 20 μm.
(F–H) SOCS1 levels in OVA-induced and control mice were analyzed by Western blot (F), IHC staining (G), and qRT-PCR (H). Scale bar: 100 μm. (n = 5).
(I) The protein levels of SOCS1 in IL-13 (100 ng/mL, 72 h) and PBS-treated hAOs were analyzed by Western blot.
(J) The mRNA levels of SOCS1 in the peripheral blood of asthma patients (n = 56) and healthy control (n = 25) were examined by qRT-PCR. Data were normalized to GAPDH mRNA.
***P < 0.001, ****P < 0.0001. (For interpretation of the references to colour in this figure legend, the reader is referred to the Web version of this article.)

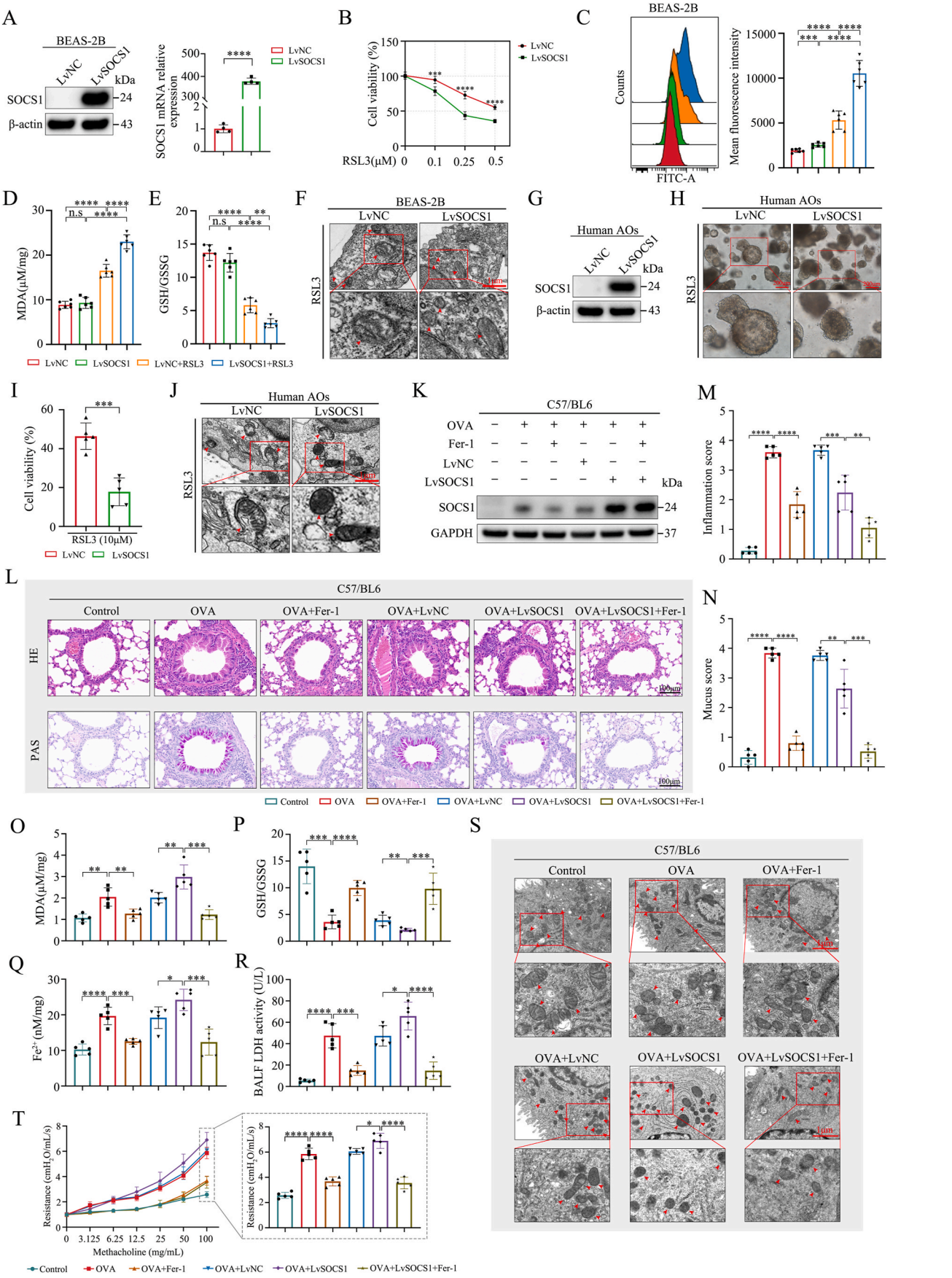

(caption on next page)

Fig. 4. SOCS1 facilitates RSL3-induced ferroptosis in airway epithelial cells.
(A) BEAS-2B cells infected with lentivirus harboring a vector encoding SOCS1 (LvSOCS1) or the empty vector (LvNC). Western blot (left panel) and qRT-PCR (right panel) were performed to detect the expression of SOCS1 (n = 4).
(B) The SOCS1-overexpressing BEAS-2B cells were treated with RSL3 at various concentrations (0, 0.1, 0.25, and 0.5 μM). The cell viability was measured by a CCK-8 kit (n = 6).
(C–E) The SOCS1-overexpressing BEAS-2B cells were treated with 0.25 μM RSL3 for 24 h, and then lipid ROS (C), intracellular MDA (D), and the GSH/GSSG ratio (E) were assayed (n = 6).
(F) Representative TEM images of the indicated cells. Red arrows indicate mitochondria. Scale bar: 1 μm
(G) HAOs were infected with lentivirus harboring a vector encoding SOCS1 (LvSOCS1) or the empty vector (LvNC). Western blot was performed to detect the levels of SOCS1.
(H–J) SOCS1-overexpressing hAOs and the control hAOs were treated with RSL3 (10 μM) for 72 h. Morphological changes of hAOs (H). Scale bar: 200 μm. The viability of organoids was measured by a cell fluorescence analyzer (I) (n = 5). Representative TEM images (J). Red arrows indicate mitochondria. Scale bar: 1 μm.
(K) The levels of SOCS1 in indicated groups of *WT* mice were detected by western blotting.
(L) Representative H&E and PAS staining images of lung tissues in indicated mice. Scale bar: 100 μm.
(M, N) Statistical analysis charts of inflammation score (M) and mucus score (N) of lung tissues in indicated mice. (n = 5).
(O–S) MDA levels (O), GSH/GSSG ratio (P), and Fe^{2+} levels (Q) of lung tissues, the activity of LDH (R) in BALF and representative TEM images of airway epithelium cells (S) in indicated groups of mice. Scale bar: 1 μm.
(T) Changes in airway resistance in response to increasing doses of Mch was assessed *in vivo* in the indicated mice (n = 5).
*P < 0.05, **P < 0.01, ***P < 0.001, ****P < 0.0001 and n.s indicates no significance. (For interpretation of the references to colour in this figure legend, the reader is referred to the Web version of this article.)

< 0.0001). All data are representative of at least four separate experiments.

3. Results

3.1. IL-13 facilitates FINs-induced ferroptosis in airway epithelial cells

To investigate that ferroptosis is associated with Th2-high asthma, we analyzed IL-13 and MDA (a lipid peroxidation marker) levels in peripheral blood serum from 25 healthy controls and 56 asthmatics. The characteristics of the participants are listed in Table 1. As expected, serum IL-13 and MDA levels were significantly higher in the asthma group than in the control group (Fig. 1A and B). Furthermore, Pearson's correlation analysis revealed a strong correlation between the serum IL-13 and MDA levels (r = 0.844, P < 0.001) (Fig. 1C). Moreover, the MDA level was negatively associated with the FEV1 expected value (an indicator of lung function) in asthmatic patients (Fig. 1D). Together, these data suggest that ferroptosis may be involved in Th2-high asthma.

Given that IL-13 was associated with MDA levels in asthma, we next investigated whether IL-13 could enhance the effect of FINs, such as erastin or RSL3, on airway epithelial cells. Subsequently, BEAS-2B cells were pretreated with IL-13 and stimulated with erastin or RSL3 for 24 h. IL-13 pretreatment reduced BEAS-2B cell survival versus erastin or RSL3 alone (Fig. 1E, Fig. S1, and Fig. S2A). Next, we estimated the levels of L-ROS (lipid peroxidation) and MDA using BODIPY 581/591 C11 and an MDA assay kit, respectively. As shown in Fig. 1F and G and Figs. S2B and C, IL-13 treatment significantly increased the FINs-induced upregulation of L-ROS and MDA levels in BEAS-2B cells. Consistently, the FINs-induced decrease in the ratio of reduced/oxidized glutathione (GSH/GSSG) (a biomarker of predictable cellular redox homeostasis) was enhanced by IL-13 treatment (Fig. 1H, Fig. S2D). Electron microscopy revealed that the morphology of ferroptotic cells was characterized by the shrinkage of mitochondria and an increase in mitochondrial intimal density. FINs-mediated morphological manifestations related to ferroptosis in the mitochondria were enhanced by IL-13 treatment (Fig. 1I, Fig. S2E). Consistent with this effect, we also observed that IL-13 promoted RSL3-induced ferroptosis in NCI–H292 cells (Fig. S2F-J). These findings together demonstrate that IL-13 might increase the sensitivity of airway epithelial cells to FINs.

Next, we established an asthma model to investigate the role of IL-13 in ferroptosis. As shown in Fig. S3A, OVA/alum-sensitized C57BL/6 mice (*WT*) and IL-13 KO (*Il-13*$^{-/-}$) mice were challenged with OVA. As expected, the enhanced infiltration of inflammatory cells (Fig. 1J, Fig. S3B), mucus secretion (Fig. 1J, Fig. S3C), AHR (Fig. 1K), and IL-13 levels (Fig. S3D) in the OVA-induced asthma mouse model were suppressed by IL-13 knockout. Notably, the elevated MDA level, decreased GSH/GSSG ratio, and increased ferrous iron level in the lung tissues of the OVA group were reversed by knockout of IL-13 (Fig. 1L-N), suggesting that IL-13 induced ferroptosis may play an important role in asthma. This notion was further confirmed by our observations that OVA-induced ferroptotic mitochondrial changes and the decreased cell viability in airway epithelial cells were alleviated by IL-13 depletion (Fig. 1O, Fig. S3E). Taken together, these findings indicate that IL-13 is an inducer of ferroptosis in airway epithelial cells in asthma.

3.2. IL-13 increases the sensitivity of hAOs to FINs

Recent progress in stem cell research has allowed for the growth of 3D organoids *in vitro*, which can mimic the structure, function, and genetic characteristics of original tissues [27]. To verify the pro-ferroptosis effects of IL-13 in airway epithelial cells and asthmatic mice models induced by OVA, we established hAOs using hESC line H9. The process of organoid establishment is shown in Fig. 2A, and images were taken every other day after resuscitation to assess their growth (Fig. 2B). Our hAOs demonstrated a round shape with thick walls and a central lumen, similar to previously described normal lung organoids [28]. We confirmed the presence of goblet and ciliated cells using immunofluorescence (Fig. 2C) and observed pseudostratified epitheliums in hAOs using H&E staining (Fig. 2D). We successfully established the hAOs and proceeded to pretreat them with IL-13 for three days and stimulated them with 10 μM RSL3 for another three days (Fig. S4). RSL3 treatment destroyed the organoid's structure, resulting in round cells that detached from the organoids; this effect was dramatically enhanced by IL-13 pretreatment (Fig. 2E). We also detected the cell viability of hAOs in response to IL-13 and/or RSL3, and the result showed that IL-13 significantly increased RSL3-induced cell death in hAOs (Fig. 2F). We observed alterations in mitochondrial ultrastructure under a transmission electron microscope, and we found that IL-13 exacerbated RSL3-induced ferroptotic mitochondrial changes in hAOs (Fig. 2G). In summary, these findings suggest that IL-13 increases the sensitivity of hAOs to FINs.

3.3. IL-13 enhances SOCS1 expression by activating STAT6

IL-13-treated BEAS-2B cells and the control cells were subjected to RNA-Seq analysis to explore the underlying mechanisms by which IL-13 regulates ferroptosis in airway epithelial cells. A total of 79 genes met the specified criteria for differentially expressed genes (DEGs), including 56 upregulated and 23 downregulated genes (Fig. 3A). To further narrow the candidate genes, a Venn diagram of these DEGs, the DEGs in the GSE37693 (IL-13-stimulated primary human airway epithelial cells) dataset, and ferroptosis-related genes (http://www.zhounan.org/ferrdb

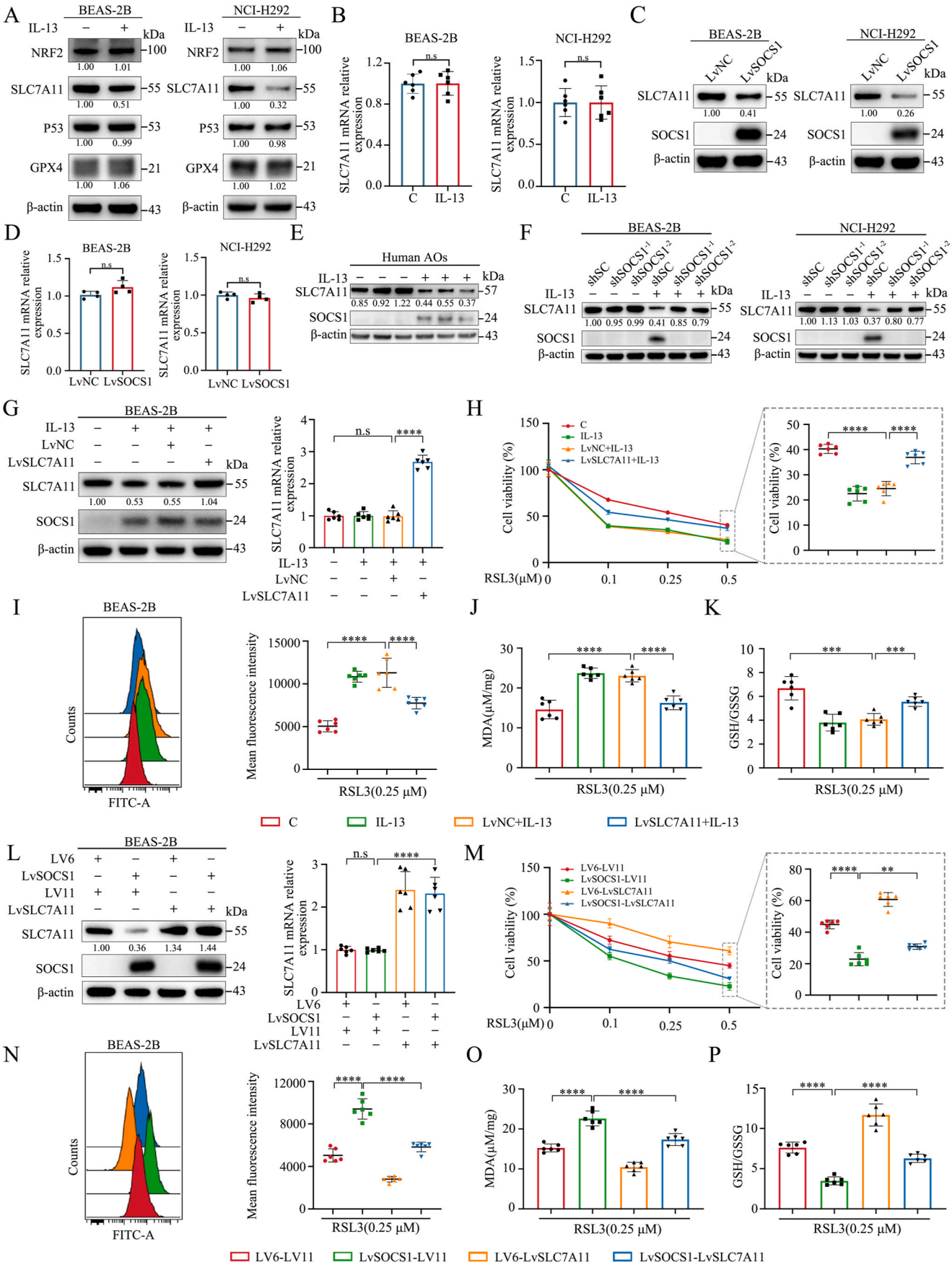

(caption on next page)

Fig. 5. The IL-13/SOCS1 pathway promotes ferroptosis through suppression of SLC7A11.
(A, B) IL-13 (100 ng/mL, 72 h) treated BEAS-2B and NCI–H292 cells were subjected to western blotting analysis with the indicated antibodies (A) and qRT-PCR analysis of SLC7A11 mRNA (B) (n = 6).
(C, D) The levels of SLC7A11 in SOCS1-overexpressing BEAS-2B and NCI–H292 cells and the corresponding control cells were measured by Western blot (C) and qRT-PCR (D) (n = 4).
(E) The protein levels of SLC7A11 in IL-13 treated hAOs were detected by immunoblotting.
(F) BEAS-2B and NCI–H292 cells with stable knockdown of SOCS1 were treated with IL-13 (100 ng/mL, 72 h). The level of SLC7A11 was examined by Western blot.
(G, L) BEAS-2B cells (G), LvSOCS1 BEAS-2B cells and the control cells (LV6) (L) were infected with lentivirus harboring a vector encoding SLC7A11 (LvSLC7A11) or the empty vector (LV11). The indicated cells were stimulated by 100 ng/mL IL-13 for 72 h (G). The levels of SLC7A11 were detected by Western blot (left panel) and qRT-PCR (right panel) (n = 6).
(H, M) Cell viability of the indicated cells treated with RSL3 at various concentrations (0, 0.1, 0.25, and 0.5 μM) was measured by a CCK-8 kit (n = 6).
(I–K, N–P) Lipid ROS levels (I, N), MDA levels (J, O) and GSH/GSSG ratio (K, P) of the indicated cells were determined (n = 6).
*P < 0.05, **P < 0.01, ***P < 0.001, ****P < 0.0001 and n.s indicates no significance.

/current/) was constructed. Only one candidate gene, SOCS1, was screened (Fig. 3B). Western blotting and qRT-PCR analyses confirmed the upregulation of SOCS1 expression in response to IL-13 administration in both BEAS-2B and NCI–H292 cells (Fig. 3C and D). Furthermore, IF verified that the expression of SOCS1 was significantly increased in BEAS-2B and NCI–H292 cells after treatment with IL-13 (Fig. 3E). We also observed that SOCS1 expression is significantly upregulated in the lung tissues of OVA-mediated asthma mice versus that in those of control mice (Fig. 3F–H). Concordantly, IL-13 activated SOCS1 expression in hAOs (Fig. 3I). In addition, we examined the mRNA level of SOCS1 in peripheral blood samples from 56 asthma patients and 25 healthy controls, as mentioned in Fig. 1A and B. The result demonstrated that the SOCS1 mRNA level in the asthma group was significantly higher than that in the control group (Fig. 3J). In summary, these results indicate that IL-13 treatment upregulates SOCS1 expression *in vitro* and *in vivo*.

STAT6, a member of the STAT family, has been shown to play a critical role in IL-13 signaling [29,30]. Indeed, IL-13 treatment led to a dramatic activation of STAT6 (Fig. S5A). Inhibition of STAT6 activity using AS1517499, a specific STAT6 inhibitor, dramatically decreased IL-13 induced SOCS1 expression in BEAS-2B cells (Fig. S5A). Similarly, interference with STAT6 using three independent siRNAs (siSTAT6^{-1}, siSTAT6^{-2}, and siSTAT6^{-3}) also significantly attenuated the stimulatory effect of IL-13 on SOCS1 expression (Fig. S5B). A ChIP-Atlas database (http://chip-atlas.org) analysis revealed that STAT6 can bind to the promotor region of the SOCS1 gene in Th1 cells, Th9 cells, and macrophages (Fig. S5C). Furthermore, three putative STAT6 binding sites (site 1: 5′-GTCAAGGAGCCTTTG-3′, −674 to −660; site 2: 5′-GGGTTCCTCTGAAGC-3′, −630 to −616; site 3: 5′-CGCTTCCCGGGAAGC-3′, −600 to −586) within a 2.0 kb region upstream of the transcription start site (TSS) of the SOCS1 gene were identified using the Jaspar database (http://jaspar.genereg.net) (Fig. S5D-F). Fragments from −849 to +184 were fused to a firefly luciferase gene lacking a promoter to generate the SOCS1-luc reporter. The recombinant reporter plasmids were co-transfected into HEK-293T cells with the internal control plasmid pRL-TK. IL-13 treatment significantly increased the luciferase activity of the reporter, whereas the enhanced transcriptional activity was attenuated when sites 1 and 3 were mutated but not when site 2 was mutated (Fig. S5G). Thus, we proposed that IL-13 promotes the expression of SOCS1 in airway epithelial cells by activating STAT6.

3.4. SOCS1 promotes ferroptosis in airway epithelial cells

We established SOCS1-overexpressing BEAS-2B and NCI–H292 cells to explore the effect of SOCS1 on ferroptosis, which was confirmed by western blotting and qRT-PCR analyses (Fig. 4A, Fig. S6A). As shown in Fig. 4B and Fig. S6B, SOCS1-overexpressing cells were more sensitive to RSL3 than control cells. Consistent with this effect, SOCS1-overexpression promoted the RSL3-induced elevation of L-ROS (Fig. 4C, Fig. S6C) and MDA (Fig. 4D, Fig. S6D) levels and further decreased the GSH/GSSG ratio (Fig. 4E, Fig. S6E) in BEAS-2B cells. Furthermore, TEM showed that SOCS1-overexpressing cell lines displayed more severe mitochondrial morphological changes than the control cells in response to RSL3 treatment (Fig. 4F, Fig. S6F). SOCS1 overexpression also significantly increased ferroptotic cell death in hAOs (Fig. 4G–J). Therefore, SOCS1 can promote ferroptosis induced by RSL3 in airway epithelial cells. Next, we determined whether SOCS1 is involved in the IL-13-mediated increase in airway epithelial cell sensitivity to FINs. We generated SOCS1-KD BEAS-2B and NCI–H292 cells with two independent shRNAs (shSOCS1^{-1} and shSOCS1^{-2}), and the knockdown efficiency was confirmed by western blotting and qRT-PCR (Figs. S7A and F). Depletion of SOCS1 dramatically attenuated the IL-13-mediated enhancement of RSL3-induced cell death and lipid peroxidation (L-ROS and MDA) (Fig. S7B-D, G-J). As expected, SOCS1 knockdown ameliorated the imbalance in the redox state (the ratio of GSH/GSSG) under ferroptotic conditions (Fig. S7E-K).

Subsequently, we established a SOCS1-overexpressing mouse model to investigate the causal role of SOCS1 and ferroptosis in OVA-induced asthma. As shown in Fig. S8, OVA-induced mice, pretreated with Fer-1 (5 mg/kg), were intratracheally administered with SOCS1-overexpressing and control lentiviruses. A noteworthy observation emerged as SOCS1 overexpression enhanced OVA-induced ferroptosis in airway epithelial cells, including elevated MDA and Fe^{2+} levels, decreased GSH/GSSG ratio in the lung tissues, increased LDH levels in BALF, exacerbated ferroptotic mitochondrial alterations, and airway hyperresponsiveness (Fig. 4K-T). Obviously, these detrimental effects were reversed by the administration of the ferroptosis inhibitor, Fer-1 (Fig. 4K-T). Collectively, these findings indicate that SOCS1 plays an important role in IL-13-promoted ferroptosis of airway epithelial cells.

3.5. The IL-13/SOCS1 pathway promotes ferroptosis by suppressing of SLC7A11

We analyzed several key proteins associated with ferroptosis (NRF2, SLC7A11, P53, and GPX4) after IL-13 exposure by western blotting to gain insight into how ferroptosis is regulated by the IL-13/SOCS1 pathway in airway epithelial cells. Notably, only SLC7A11 was significantly downregulated in response to IL-13 treatment in BEAS-2B and NCI–H292 cells (Fig. 5A). Interestingly, IL-13 had little effect on SLC7A11 mRNA expression (Fig. 5B), suggesting that IL-13 regulates SLC7A11 at the protein level. In line with IL-13 treatment, overexpression of SOCS1 downregulated SLC7A11 at the protein level, but not mRNA expression in BEAS-2B and NCI–H292 cells (Fig. 5C and D). Additionally, the protein level of SLC7A11 was dramatically decreased in hAOs upon IL-13 treatment (Fig. 5E). Importantly, SOCS1 knockdown compromised the IL-13-induced inhibition of SLC7A11 in BEAS-2B and NCI–H292 cells (Fig. 5F). Together, these data indicate that IL-13 inhibits the protein level of SLC7A11 by upregulating of SOCS1 expression.

To investigate whether SLC7A11 is involved in ferroptosis regulated by the IL-13/SOCS1 pathway, we established SLC7A11-overexpressing cell lines to detect its influence on ferroptosis with IL-13 treatment. As shown in Fig. 5G–K and Fig. S9A-E, overexpressing of SLC7A11 alleviated the enhanced ferroptosis induced by IL-13, decreasing in cell death,

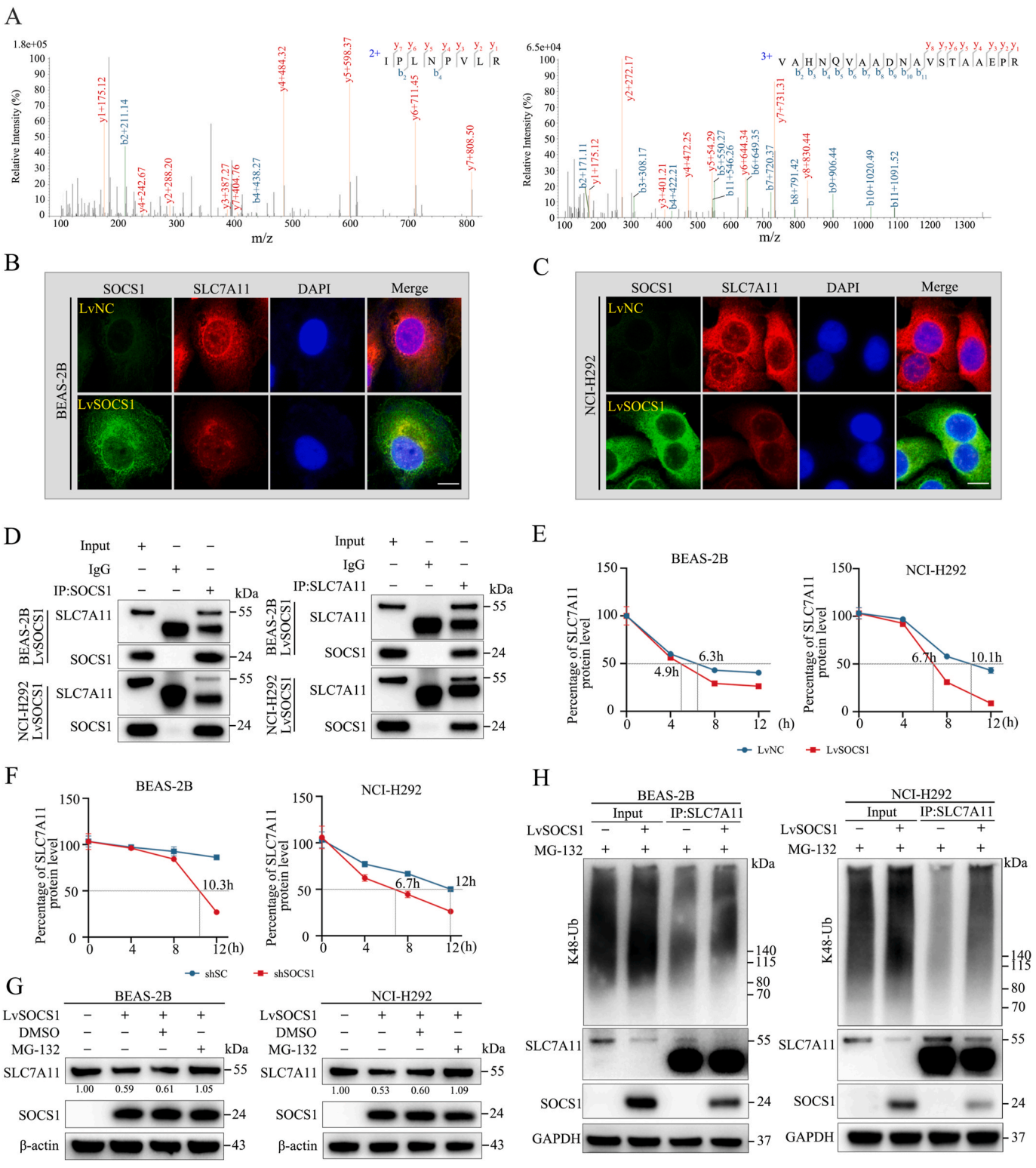

Fig. 6. SOCS1 promotes the ubiquitinated degradation of SLC7A11.

(A) Secondary mass spectra images of the unique peptides of SOCS1.

(B, C) Representative IF images of SOCS1 and SLC7A11 in LvSOCS1 or LvNC BEAS-2B (B) and NCI–H292 cells (C). Nuclei were stained with DAPI (× 10). Scale bar: 10 μm.

(D) Co-IP and Western blot assay were performed to detect SOCS1 and SLC7A11 proteins in SOCS1-overexpressing BEAS-2B and NCI–H292 cells.

(E, F) Statistical analysis charts of SLC7A11 protein degradation in indicated cells according to Western blot assay (Figs. S10C and D).

(G) After exposed to MG-132 (10 μM) for 6 h, the levels of SLC7A11 in indicated cells were detected by Western blot.

(H) SLC7A11 polyubiquitination was detected by anti-K48-Ub immunoblotting in SOCS1-overexpressing BEAS-2B and NCI–H292 cells.

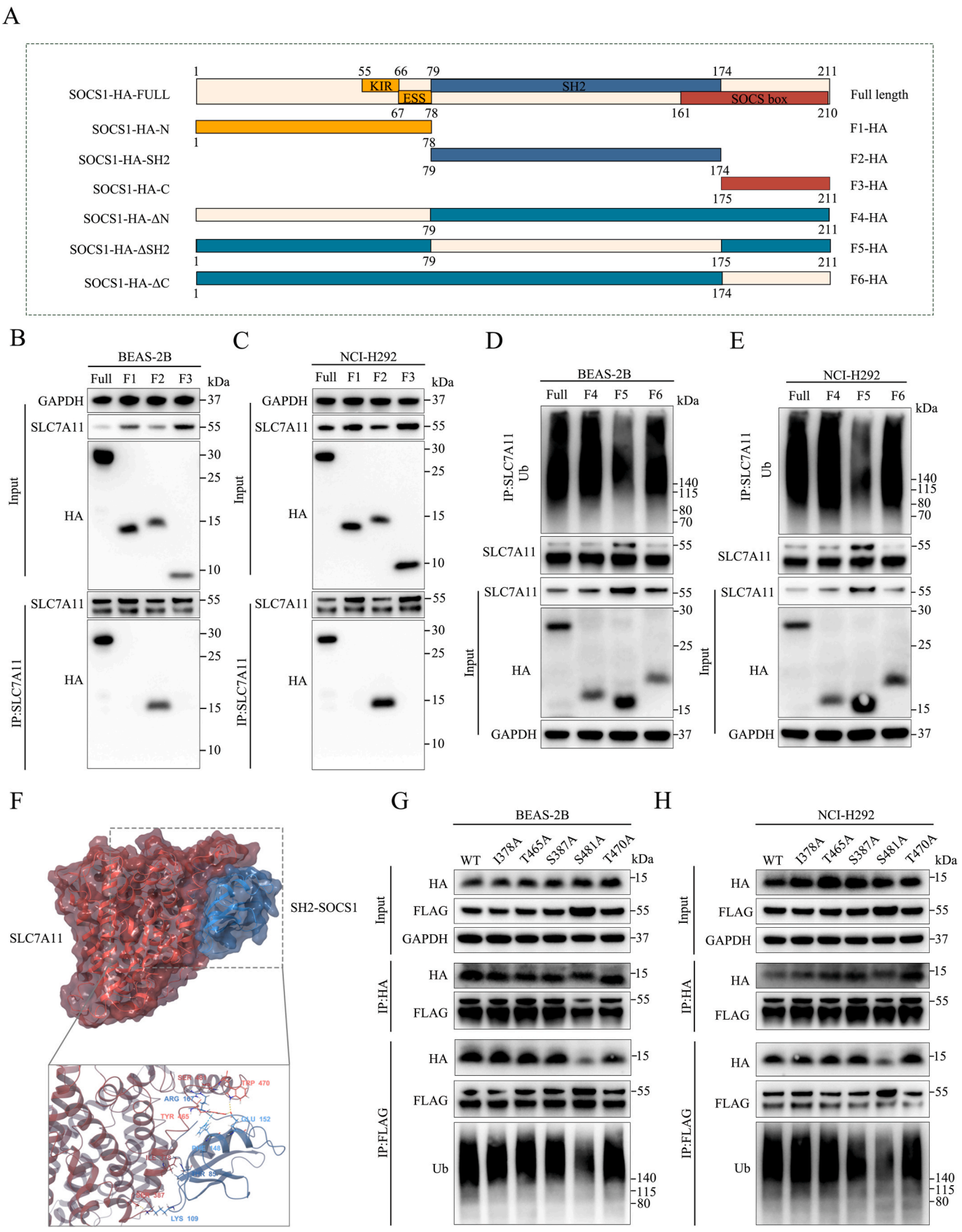

(caption on next page)

Fig. 7. The SH2-domain of SOCS1 binds to SLC7A11 and promotes its ubiquitination.
(A) Diagram of the different domains of the SOCS1 constructs and truncated plasmids.
(B, C) Co-IP assay to assess the interaction between SLC7A11 and different domains of SOCS1. Full length of SOCS1, F1-HA (SOCS1-HA-N), F2-HA (SOCS1-HA-SH2), and F3-HA (SOCS1-HA-C) plasmids were transfected into BEAS-2B (B) and NCI–H292 (C) cells. The cell lysates were immunoprecipitated with SLC7A11 and then subjected to Western blot analysis using anti-HA.
(D, E) Ubiquitination assay to detect the ubiquitination level of SLC7A11 in BEAS-2B (D) and NCI–H292 (E) cells, transfected with full length of SOCS1, F4-HA (SOCS1-HA-ΔN), F5-HA (SOCS1-HA-ΔSH2), and F6-HA (SOCS1-HA-ΔC) plasmids.
(F) Molecular docking model of SLC7A11 (red) interacting with the SH2-domain of SOCS1 (blue).
(G, H) Co-IP and ubiquitination assay to identify the amino acid sites of SLC7A11 binding to SOCS1 in BEAS-2B (G) and NCI–H292 cells (H), with different SLC7A11 mutants. The immunoprecipitates were analyzed by Western blot using an anti-HA antibody and anti-Flag antibody. (For interpretation of the references to colour in this figure legend, the reader is referred to the Web version of this article.)

intracellular L-ROS and MDA production, and increasing the GSH/GSSG ratio. Similar effects were observed in SOCS1-overexpressing BEAS-2B and NCI–H292 cells when of SLC7A11 was re-introduced (Fig. 5L-P, Fig. S9F-J). Thus, IL-13/SOCS1 pathway facilitates ferroptosis by suppressing of SLC7A11.

3.6. SOCS1 promotes the ubiquitinated degradation of SLC7A11

Since SOCS1 is a member of the SOCS family and has been shown to function as an E3 ubiquitin ligase [31,32], we wondered whether SOCS1 could interact directly with SLC7A11 to promote its ubiquitinated degradation. Subsequently, we performed an immunoprecipitation assay using anti-SLC7A11 and IgG agarose beads in BEAS-2B cells stably overexpressing SOCS1. Mass spectrometry analysis was used to identify the proteins that potentially interacted with SLC7A11 (Fig. S10A). Strikingly, this analysis identified 2 unique peptides corresponding with SOCS1, "IPLNPVLR" and "VAHNQVAADNAVSTAAEPR" (Fig. S10B), indicating that SLC7A11 can bind to SOCS1. The secondary mass spectra of these unique peptides are shown in Fig. 6A. Furthermore, IF staining verified that SOCS1 and SLC7A11 were mainly cytoplasmic co-expression in BEAS-2B and NCI–H292 cells (Fig. 6B and C). Notably, the expression levels of SLC7A11 had significant negative correlations between SOCS1 (Fig. 6B and C). Afterwards, BEAS-2B or NCI–H292 cells stably overexpressing SOCS1 were assessed by co-IP using anti-SOCS1 and anti-SLC7A11 agarose beads to further validate the interaction between SOCS1 and SLC7A11. The results confirmed that SOCS1 could specifically and directly bind to SLC7A11 (Fig. 6D). Next, we determined whether SOCS1 could induce SLC7A11 degradation. As shown in Fig. S10C and Fig. 6E, the steady-state level of SLC7A11 was markedly reduced after SOCS1 overexpression, and the half-life of SLC7A11 was considerably shortened. In contrast, the steady-state level and half-life of the SLC7A11 protein were considerably extended in SOCS1-KD cells (Fig. 6F, Fig. S10D). Therefore, SOCS1 inhibited SLC7A11 expression by promoting its protein degradation. To further investigate the underlying mechanism of SLC7A11 degradation, we treated BEAS-2B and NCI–H292 cells with a proteasome inhibitor (MG-132) and a lysosome inhibitor (leupeptin). Notably, SOCS1 overexpression-mediated SLC7A11 degradation was blocked by pretreatment with MG-132 but not leupeptin (Fig. 6G, Fig. S10E), suggesting that SOCS1 suppresses the proteasomal degradation of SLC7A11 without affecting its degradation via the lysosomal pathway. Since SOCS1 is an E3 ubiquitin ligase and interacts with SLC7A11, we speculated that SLC7A11 might be a substrate of SOCS1. In line with this premise, a more pronounced level of K48-linked ubiquitination of SLC7A11 was observed in SOCS1-overexpressing BEAS-2B and NCI–H292 cells (Fig. 6H). Collectively, the above findings suggest that SOCS1 binds to SLC7A11 directly, increasing the ubiquitination and degradation of SLC7A11.

3.7. The SH2-domain of SOCS1 interacts with SLC7A11 and promotes its ubiquitination

To clarify the domain of SOCS1 that interacts with SLC7A11, we constructed full-length (Full-HA) and truncated plasmids [(F1:SOCS1-HA-N (1–78), F2:SOCS1-HA-SH2 (79–174), and F3:SOCS1-HA-C (175–211))] based on the structural domain sequences of SOCS1 with 3 × HA tags at the C-termini and transfected these plasmids into BEAS-2B and NCI–H292 cells. The schematic map of the constructed plasmids is presented in Fig. 7A. The co-IP assay illustrated that SLC7A11 selectively binds to the SH2-domain of SOCS1 (Fig. 7B and C). Subsequently, to investigate the impact of different SOCS1 domains on the level of ubiquitination, we constructed three domain-deleted plasmids (F4: SOCS1-HA-ΔN, F5:SOCS1-HA-ΔSH2, and F6:SOCS1-HA-ΔC), as illustrated in Fig. 7A. Ubiquitination assays showed deleting the SH2-domain of SOCS1 (SOCS1-HA-ΔSH2) markedly decreased the SLC7A11 ubiquitination level compared with that observed with the full-length SOCS1 (Fig. 7D and E). Therefore, SOCS1 induces SLC7A11 ubiquitination through the SH2-structural domain of SOCS1.

A molecular docking model was used to predict the binding of the SH2-domain of SOCS1 (Set 1) residues to SLC7A11 (Set 2) to further identify the structural domain of SLC7A11 interacting with SOCS1. The molecular docking results are shown in Table S3, revealing that SLC7A11 binds to the SH2-structural domain of SOCS1 through H-bonds and van der Waals at sites including Ile378, Tyr465, Ser387, Ser481, and Trp470 (Fig. 7F). Accordingly, we constructed five SLC7A11 mutants for co-IP: I378A, T465A, S387A, S481A, and T470A. Co-IP and ubiquitination assays showed that mutating the S481 residue to A481 destroyed the binding of SLC7A11 to SOCS1 and decreased the SLC7A11 ubiquitination level (Fig. 7G and H). In contrary, the other mutations in SLC7A11 did not significantly affect the interaction between SLC7A11 and SOCS1 or the ubiquitination level of SLC7A11. In summary, our results indicate that the SH2-domain of SOCS1 interacts with Ser481 of SLC7A11 and promotes the ubiquitination and degradation of SLC7A11.

3.8. SOCS1 promotes ferroptosis of the bronchial epithelium and enhances AHR in IL-13-related asthmatic mice

WT mice were intratracheally administered SOCS1 siRNA or control siRNA and challenged with OVA to verify the importance of SOCS1 in IL-13-mediated ferroptosis in the airway epithelium *in vivo* (Fig. 8A). In line with the above *in vitro* results, the protein level of SLC7A11 was significantly decreased in the lung tissues of OVA-treated mice and increased after SOCS1 interference (Fig. 8B and C). Moreover, SOCS1 knockdown significantly decreased MDA and Fe^{2+} levels and increased the GSH/GSSG ratio in the lung tissues of the OVA-induced asthma model (Fig. 8D–F). Meanwhile, the OVA-induced elevation of LDH activity in BALF and ferroptotic mitochondrial changes in the airway epithelial cells were markedly alleviated by the depletion of SOCS1 (Fig. 8G and H). Interestingly, the inhibition of SOCS1 markedly suppressed AHR in the OVA-induced asthma model (Fig. 8I), implying that ferroptosis is involved in AHR in IL-13 related asthma.

To further explore the role of SOCS1 in IL-13-associated asthma, we intratracheally administered SOCS1-overexpression and control lentiviruses to *Il-13*$^{-/-}$ mice challenged with OVA (Fig. 8J). Expectedly, we found that the expression of SLC7A11 was not significantly reduced in OVA-challenged *Il-13*$^{-/-}$ mice, but decreased by SOCS1 overexpression (Fig. 8K and L). Accordingly, overexpression of SOCS1 resulted in elevated MDA and Fe^{2+} levels, decreased GSH/GSSG ratios in the lung tissues, increased LDH activity in BALF, and exacerbated ferroptotic

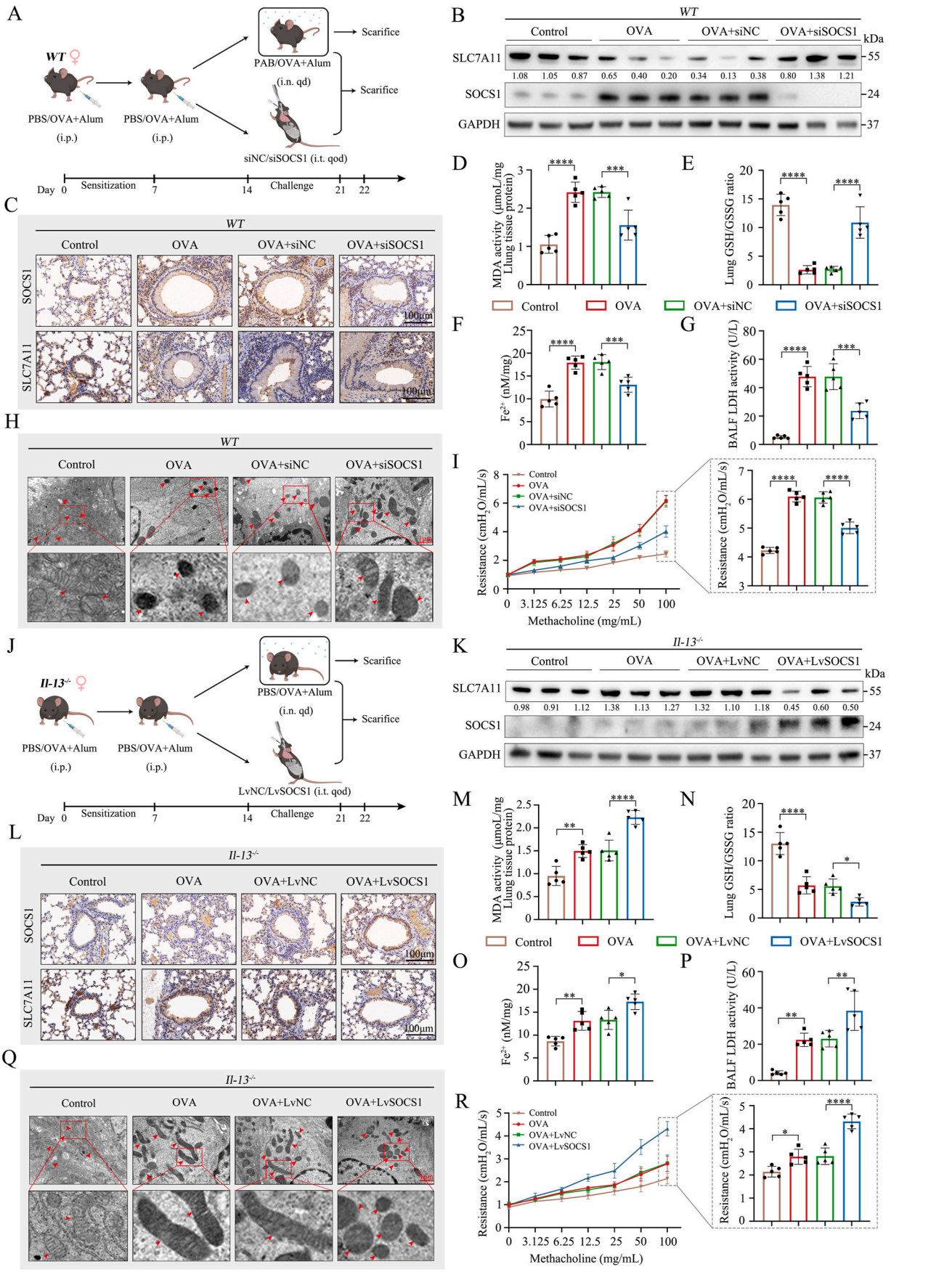

(caption on next page)

Fig. 8. SOCS1 promotes ferroptosis of the bronchial epithelium and enhances AHR in IL-13-related asthma mice.
(A, N) Establishment of OVA-induced asthma mouse model and schedule of therapeutic intervention in *WT* C57/BL6 mice (A) and *Il-13*$^{-/-}$ C57/BL6 mice (N).
(B, C, K and L) The levels of SLC7A11 and SOCS1 in indicated groups of *WT* and *Il-13*$^{-/-}$ mice were detected by western blotting (B, K) and IHC staining (C, L). Scale bar: 100 μm.
(D-H, M-Q) MDA levels (D, M) and GSH/GSSG ratio (E, N) and Fe^{2+} levels (F, Q) of lung tissues, LDH activity in BALF (G, P) and representative TEM images of airway epithelium cells (H, Q) in indicated groups of mice. Scale bar: 1 μm.
(I, R) Changes in airway resistance in response to increasing doses of Mch was assessed *in vivo* in the indicated mice.
The data represent means ± SEM from 5 mice per group.
*P < 0.05, **P < 0.01, ***P < 0.001, ****P < 0.0001 and n.s indicates no significance.

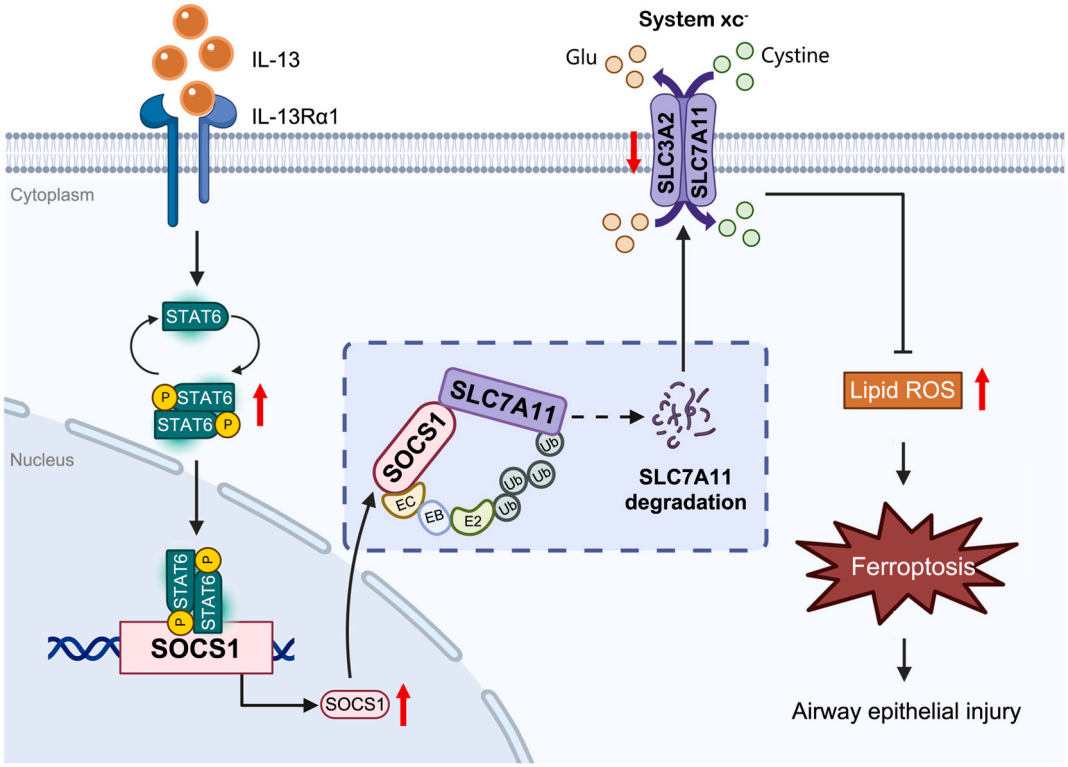

Fig. 9. Schematic illustration of IL-13 facilitates ferroptotic death in asthmatic epithelial cells through the STAT6/SOCS1/SLC7A11 signaling pathway.

mitochondrial alterations in airway epithelial cells (Fig. 8M-Q). Meanwhile, the ectopic expression of SOCS1 increased AHR in *Il-13*$^{-/-}$ mice (Fig. 8R). These findings suggest that SOCS1 can induce ferroptosis and AHR in IL-13 related asthma mice.

4. Discussion

Emerging evidence indicates that ferroptosis plays a critical role in the development of Th2-high asthma [19,20,33,34]; however, the underlying mechanisms are largely unclear. In this study, we explored how IL-13 promotes ferroptosis in Th2-high asthma using clinical samples, airway epithelial cells, hAOs, and the OVA-induced asthma mouse model. First, we found that the serum MDA level, a lipid peroxidation marker, was positively associated with IL-13 but negatively with FEV1% in asthma patients. Second, we found that IL-13 promoted ferroptosis in airway epithelial cells by upregulating SOCS1 expression. Finally, we showed that SOCS1 directly binds with SLC7A11 and accelerates its ubiquitinated degradation, leading to ferroptosis in airway epithelial cells. Our findings not only uncover a novel regulatory mechanism by which IL-13 induces ferroptosis in airway epithelial cells, but also, for the first time, link the ferroptosis of airway epithelial cells to AHR in Th2-high asthma. Together with previous findings that IL-13 can promote ferroptotic death in asthmatic epithelial cells through an increase in the colocalization of 15LO1 and PEBP1 [33,35], our findings suggest that inhibiting the ferroptosis of airway epithelial cells may be an effective treatment strategy for Th2-high asthma.

Obtaining lung tissue from asthma patients is difficult for ethical reasons. Immortalized airway epithelial cells are widely used to study asthma due to ease of culture and low cost [7,36,37]. However, these cell lines can only be cultured in a single layer, and it is difficult to imitate the influence of the specific structure of the human airway epithelium, that is, the pseudostratified ciliated epithelial structure, on the occurrence and development of asthma. Several animal asthma models have been developed and used to simulate the effects of allergens, pathogens, or cytokines on airway epithelial cells, which still have certain limitations [38]. For example, there are many inherent differences between human and mouse lung tissues, such as the basal cells that are present only in the trachea in mice but exist throughout the airway in humans [39]. Thus, it is critical to develop novel models to investigate the mechanism of asthma. In this study, we established hAOs through stem cell-induced differentiation. Furthermore, we identified that the most characteristic cells of these airway organoids are ciliated cells and mucous-secreting cells. Moreover, H&E staining demonstrated that hAOs have the characteristic pseudostratified ciliated epithelial structure. These findings indicate that the hAOs we established have a similar structure to the human respiratory tract. Consistent with the findings in airway epithelium cells and mouse models, we confirmed the critical role of the IL-13/SOCS1 pathway in ferroptosis using the hAOs model. Therefore, hAOs established from stem cells are effective models for studying Th2-high asthma. We will further explore and optimize the

culture of airway organoids in the future, for example, by establishing hAOs derived from lung tissues and screening and identifying of valgus-type and varus-type airway organoids.

SOCS1, the most important of the eight SOCS family members, comprises a central SH2-domain and a SOCS box [40]. It is well-known that SOCS1 can inhibit inflammation by enhancing the ubiquitinated degradation of JAK, leading to the suppression of the phosphorylation of STAT family proteins [32]. Relevant studies have demonstrated that SOCS1 is elevated in Th2-high inflammation states, including, allergic rhinitis [41], asthma [42], and atopic dermatitis [43]. Thus, SOCS1 likely plays a protective role in Th2-high inflammation [44,45]. Consistent with this idea, we observed that SOCS1 overexpression inhibited airway inflammation in the OVA-induced mouse model but significantly enhanced AHR. Consistently, Gielen et al. observed that SOCS1 levels are positively associated with AHR in asthmatic patients [42]. Furthermore, we found extensive evidence that SOCS1 promotes ferroptosis in airway epithelial cells. First, overexpression of SOCS1 induced ferroptosis in BEAS-2B and NCI–H292 cells, hAOs, and OVA-challenged mice. Meanwhile, Fer-1 can reverse the exacerbation of ferroptosis and AHR in airway epithelial cells caused by SOCS1 overexpression in OVA-induced *WT* mice. Second, knockdown of SOCS1 rescued, at least in part, the IL-13-induced ferroptosis in BEAS-2B and NCI–H292 cells, and alleviated the ferroptotic cell death of airway epithelial cells in OVA-induced asthmatic mice. Interestingly, the link between SOCS1 and ferroptosis has been observed in other cell models in which interference of SOCS1 with SOCS1 siRNA could inhibit baicalin-induced ferroptosis in hepatic stellate cells [46]. Therefore, it is possible that SOCS1-mediated ferroptosis in airway epithelial cells is a leading cause of AHR in Th2-high asthma.

SLC7A11, a critical regulator of ferroptosis, has been demonstrated to participate in the development of various diseases [47–50]. Thus, it is important to examine how SLC7A11 expression is controlled. Several transcription factors have been demonstrated to regulate the transcription of the SLC7A11 gene, such as NRF2 [51,52], ATF4 [47], and p53 [53]. Meanwhile, SLC7A11 can be regulated at the posttranscriptional level by some RNA binding proteins and non-coding RNAs, including RBMS1 [54], IGF2BP1 [55], and miR-5096 [56]. Recent studies have suggested that some molecules, such as OTUB1 [57] and BAP1 [58], can influence the stability of the SLC7A11 protein through ubiquitinated degradation. Herein, we demonstrated that SOCS1, an E3 ubiquitin ligase, promotes the proteasomal degradation of SLC7A11 by catalyzing its ubiquitination. Mechanistically, we showed that the SH2-domain of SOCS1 binds with SLC7A11-Ser481 (located in the C-terminal) and then induces the ubiquitinated degradation of SLC7A11. Our work not only identifies a new target of SOCS1, but also enriches the understanding of SLC7A11 regulation. Interestingly, a recent study demonstrated that another member of the SOCS family, SOCS2 can promote the ubiquitinated degradation of SLC7A11 in hepatocellular carcinoma cells [59]. In that study, the N-terminal domain of SLC7A11 was found to bind to the SH2-domain of SOCS1 as opposed to the C-terminal domain binding observed here. This phenomenon is not rare. For example, TRIM27 and TRIM8, two members of the TRIM family, interact with and activate TAK1 at different domains [60,61].

Despite the strengths of this study, two limitations should be acknowledged. First, MDA assay is indeed defective due to the fact that TBA could easily react with other cellular substrates that can drastically increase the levels of product in this assay [62]. Therefore, other ferroptosis-related indicators, such as the morphological changes of mitochondrial in the airway epithelial cells of asthmatic patients, the ratio of GSH/GSSG, and ferrous iron content in the body fluid, could be included to reflect the ferroptosis level of asthmatic patients. In the future, we will collect fresh plasma and BALF of asthmatic patients and employ above complementary approaches to address this issue. Second, knockdown of SOCS1 could not fully reverse the downregulation of SLC7A11 induced by IL-13, suggesting that other signaling molecules may also be involved in the regulation of SLC7A11 downstream of IL-13. We will further investigate the issue in future work.

5. Conclusions

In summary, our findings demonstrate that IL-13 upregulates SOCS1 by activating STAT6, which in turn promotes ferroptosis in airway epithelial cells by directly binding to and inducing the ubiquitinated degradation of SLC7A11 in Th2-high asthma. Thus, targeting the IL-13/STAT6/SOCS1/SLC7A11 pathway in airway epithelial cells may be a novel therapeutic approach for treating Th2-high asthma (Fig. 9).

Funding

This work was supported by the National Natural Science Foundation of China (U1803126), the Anhui Provincial Natural Science Foundation (2308085MH237, 2208085MH239), the Natural Science Foundation of Universities of Anhui Province (KJ2019A0219), the Research Fund of Anhui Institute of Translational Medicine (2022zhyx-C22), the Co-construction Project of Clinical and Preliminary Disciplines of Anhui Medical University (2021lcxk005), the Academic and Technical Leaders Fund of Anhui Provincial Human Resources and Social Security Department (2020D249), the Key Program in the Youth Elite Support Plan in Universities of Anhui Province (gxyqZD2017022), and Key Projects of Academic Support for Top Talents in Colleges and Universities, China (gxbjZD2016036).

Data availability statement

The data supporting the conclusions of this article have been given in this article and its additional files.

Ethics approval and consent to participate

All donors provided written informed consent, and the peripheral blood donation of all participants was approved by the Biomedical Ethics Committee of Anhui Medical University (5101137). All animal experiments were approved by the Experimental Animal Ethical Committee of Anhui Medical University (LLSC20210231).

CRediT authorship contribution statement

Manli Miao: Formal analysis, Investigation, Writing – original draft. **Min Pan:** Formal analysis, Writing – original draft, Investigation. **Xu Chen:** Formal analysis, Investigation, Writing – original draft. **Jiapan Shen:** Investigation. **Ling Zhang:** Investigation. **Xiaoxia Feng:** Investigation. **Mengting Chen:** Investigation. **Guofeng Cui:** Investigation. **Huaiyuan Zong:** Investigation. **Wen Zhang:** Investigation. **Shuang Chang:** Investigation. **Fangzhou Xu:** Investigation. **Zixi Wang:** Formal analysis. **Dapeng Li:** Formal analysis. **Weiwei Liu:** Formal analysis. **Zhao Ding:** Formal analysis. **Shengquan Zhang:** Writing – review & editing. **Biao Chen:** Conceptualization, Writing – review & editing. **Xiaojun Zha:** Conceptualization, Funding acquisition, Writing – review & editing. **Xiaoyun Fan:** Conceptualization, Funding acquisition, Writing – review & editing.

Declaration of competing interest

The authors declare that there are no conflicts of interests.

Acknowledgments

We thank Yufei Xu, Xueqin Jiang, and Xiaoyan Han (Department of Geriatric Respiratory and Critical Care Medicine, the First Affiliated Hospital of Anhui Medical University, Hefei, China) for collecting clinical specimens. We thank all the patients that participated in this study. We thank for the support of Center for Scientific Research, Anhui

Medical University. We thank LetPub (https://www.letpub.com) for its linguistic assistance during the preparation of this manuscript. We thank BioRender (https://www.biorender.com/) for assisting in drawing graphical abstract.

Abbreviations

IL-13	Interleukin 13
MDA	Malondialdehyde
FEV1%	The predicted forced expiratory volume in 1 s
SOCS1	Suppressor of cytokine signaling 1
hAOs	Human airway organoids
OVA	Ovalbumin
STAT6	Signal transducer and activator of transcription 6
GPX4	Glutathione peroxidase 4
KO	Knockout
FINs	Ferroptosis inducers
SLC7A11	Solute carrier family 7 member 11
AHR	Airway hyperresponsiveness
GINA	Global Initiative for Asthma
LPOs	Lung bud tip progenitor organoids
DMEM	Dulbecco's modified Eagle's medium
RPMI	Roswell Park Memorial Institute
FBS	Fetal bovine serum
hESC	Human embryonic stem cell
BSA	Bovine serum albumin
AO/PI	Acridine orange and propidium iodide
HHT	Homoharringtonine
DMSO	Dimethyl sulfoxide
GAPDH	Glyceraldehyde 3-phosphate dehydrogenase
KD	Knockdown
shRNA	Short hairpin RNA
RNA-Seq	High-throughput RNA sequencing
DEGs	Differentially expressed genes
GEO	Gene Expression Omnibus
SDS-PAGE	SDS-polyacrylamide gel electrophoresis
qRT-PCR	Quantitative real-time polymerase chain reaction
cDNA	Complementary DNA
IF	Immunofluorescence
PFA	Paraformaldehyde
ELISA	Enzyme-linked immunosorbent assay
BALF	Bronchoalveolar lavage fluid
WT	Wild type
MS	Mass spectrometry
co-IP	Co-immunoprecipitation
SPF	Specific pathogen-free
MCh	Methacholine
IHC	Immunohistochemistry
H&E	Hematoxylin and eosin
PAS	Periodic acid-schiff
TEM	Transmission electron microscopy
L-ROS	Lipid peroxidation
GSH/GSSG	Glutathione/glutathione disulfide
TSS	Transcription start site

Appendix A. Supplementary data

Supplementary data to this article can be found online at https://doi.org/10.1016/j.redox.2024.103100.

References

[1] J. Stern, J. Pier, A.A. Litonjua, Asthma epidemiology and risk factors, Semin. Immunopathol. 42 (2020) 5–15, https://doi.org/10.1007/s00281-020-00785-1.
[2] C. Porsbjerg, E. Melen, L. Lehtimaki, et al., Asthma, Lancet 401 (2023) 858–873, https://doi.org/10.1016/S0140-6736(22)02125-0.
[3] K. Oh, M.W. Seo, G.Y. Lee, et al., Airway epithelial cells initiate the allergen response through transglutaminase 2 by inducing IL-33 expression and a subsequent Th2 response, Respir. Res. 14 (2013) 35, https://doi.org/10.1186/1465-9921-14-35.
[4] D.P. Potaczek, S. Miethe, V. Schindler, et al., Role of airway epithelial cells in the development of different asthma phenotypes, Cell. Signal. 69 (2020) 109523, https://doi.org/10.1016/j.cellsig.2019.109523.
[5] S.G. Royce, X. Li, S. Tortorella, et al., Mechanistic insights into the contribution of epithelial damage to airway remodeling. Novel therapeutic targets for asthma, Am. J. Respir. Cell Mol. Biol. 50 (2014) 180–192, https://doi.org/10.1165/rcmb.2013-0008OC.
[6] K.S. Schweitzer, T. Crue, J.M. Nall, et al., Influenza virus infection increases ACE2 expression and shedding in human small airway epithelial cells, Eur. Respir. J. 58 (2021), https://doi.org/10.1183/13993003.03988-2020.
[7] C. Zhao, Y. Wang, Z. Su, et al., Respiratory exposure to PM2.5 soluble extract disrupts mucosal barrier function and promotes the development of experimental asthma, Sci. Total Environ. 730 (2020) 139145, https://doi.org/10.1016/j.scitotenv.2020.139145.
[8] B.N. Lambrecht, H. Hammad, The immunology of asthma, Nat. Immunol. 16 (2015) 45–56, https://doi.org/10.1038/ni.3049.
[9] M. Jia, X. Yan, X. Jiang, et al., Ezrin, a membrane cytoskeleton cross-linker protein, as a marker of epithelial damage in asthma, Am. J. Respir. Crit. Care Med. 199 (2019) 496–507, https://doi.org/10.1164/rccm.201802-0373OC.
[10] D.A. Kuperman, X. Huang, L.L. Koth, et al., Direct effects of interleukin-13 on epithelial cells cause airway hyperreactivity and mucus overproduction in asthma, Nat. Med. 8 (2002) 885–889, https://doi.org/10.1038/nm734.
[11] T. Nagasaki, A.J. Schuyler, J. Zhao, et al., 15LO1 dictates glutathione redox changes in asthmatic airway epithelium to worsen type 2 inflammation, J. Clin. Invest. 132 (2022), https://doi.org/10.1172/JCI151685.
[12] S.J. Wadsworth, R. Atsuta, J.O. McIntyre, et al., IL-13 and TH2 cytokine exposure triggers matrix metalloproteinase 7-mediated Fas ligand cleavage from bronchial epithelial cells, J. Allergy Clin. Immunol. 126 (2010) 366–374, https://doi.org/10.1016/j.jaci.2010.05.015, 371-374.
[13] S.J. Dixon, K.M. Lemberg, M.R. Lamprecht, et al., Ferroptosis: an iron-dependent form of nonapoptotic cell death, Cell 149 (2012) 1060–1072, https://doi.org/10.1016/j.cell.2012.03.042.
[14] H.F. Yan, T. Zou, Q.Z. Tuo, et al., Ferroptosis: mechanisms and links with diseases, Signal Transduct. Targeted Ther. 6 (2021) 49, https://doi.org/10.1038/s41392-020-00428-9.
[15] T. Hong, G. Lei, X. Chen, et al., PARP inhibition promotes ferroptosis via repressing SLC7A11 and synergizes with ferroptosis inducers in BRCA-proficient ovarian cancer, Redox Biol. 42 (2021) 101928, https://doi.org/10.1016/j.redox.2021.101928.
[16] C. Bartolacci, C. Andreani, G. Vale, et al., Targeting de novo lipogenesis and the Lands cycle induces ferroptosis in KRAS-mutant lung cancer, Nat. Commun. 13 (2022) 4327, https://doi.org/10.1038/s41467-022-31963-4.
[17] M. Yoshida, S. Minagawa, J. Araya, et al., Involvement of cigarette smoke-induced epithelial cell ferroptosis in COPD pathogenesis, Nat. Commun. 10 (2019) 3145, https://doi.org/10.1038/s41467-019-10991-7.
[18] D. Yue, Q. Zhang, J. Zhang, et al., Diesel exhaust PM2.5 greatly deteriorates fibrosis process in pre-existing pulmonary fibrosis via ferroptosis, Environ. Int. 171 (2023) 107706, https://doi.org/10.1016/j.envint.2022.107706.
[19] Z. Zeng, H. Huang, J. Zhang, et al., HDM induce airway epithelial cell ferroptosis and promote inflammation by activating ferritinophagy in asthma, Faseb. J. 36 (2022) e22359, https://doi.org/10.1096/fj.202101977RR.
[20] C. Bao, C. Liu, Q. Liu, et al., Liproxstatin-1 alleviates LPS/IL-13-induced bronchial epithelial cell injury and neutrophilic asthma in mice by inhibiting ferroptosis, Int. Immunopharm. 109 (2022) 108770, https://doi.org/10.1016/j.intimp.2022.108770.
[21] Y. Wu, H. Chen, N. Xuan, et al., Induction of ferroptosis-like cell death of eosinophils exerts synergistic effects with glucocorticoids in allergic airway inflammation, Thorax 75 (2020) 918–927, https://doi.org/10.1136/thoraxjnl-2020-214764.
[22] X. Chen, M. Miao, M. Zhou, et al., Poly-L-arginine promotes asthma angiogenesis through induction of FGFBP1 in airway epithelial cells via activation of the mTORC1-STAT3 pathway, Cell Death Dis. 12 (2021) 761, https://doi.org/10.1038/s41419-021-04055-2.
[23] R. Wang, N. Kang, W. Zhang, et al., The developmental toxicity of PM2.5 on the early stages of fetal lung with human lung bud tip progenitor organoids, Environ. Pollut. 330 (2023) 121764, https://doi.org/10.1016/j.envpol.2023.121764.
[24] D. Li, A. Sun, L. Zhang, et al., Elevated ITGA5 facilitates hyperactivated mTORC1-mediated progression of laryngeal squamous cell carcinoma via upregulation of EFNB2, Theranostics 12 (2022) 7431–7449, https://doi.org/10.7150/thno.76232.
[25] H. Li, P. Liu, D. Li, et al., STAT3/miR-130b-3p/MBNL1 feedback loop regulated by mTORC1 signaling promotes angiogenesis and tumor growth, J. Exp. Clin. Cancer Res. 41 (2022) 297, https://doi.org/10.1186/s13046-022-02513-z.
[26] M. Guan, H. Ma, X. Fan, et al., Dexamethasone alleviate allergic airway inflammation in mice by inhibiting the activation of NLRP3 inflammasome, Int. Immunopharm. 78 (2020) 106017, https://doi.org/10.1016/j.intimp.2019.106017.
[27] J. Kim, B.K. Koo, J.A. Knoblich, Human organoids: model systems for human biology and medicine, Nat. Rev. Mol. Cell Biol. 21 (2020) 571–584, https://doi.org/10.1038/s41580-020-0259-3.
[28] N. Sachs, A. Papaspyropoulos, O.D. Zomer-van, et al., Long-term expanding human airway organoids for disease modeling, EMBO J. 38 (2019), https://doi.org/10.15252/embj.2018100300.

[29] J.R. Cortes, M.D. Rivas, J. Molina-Infante, et al., Omeprazole inhibits IL-4 and IL-13 signaling signal transducer and activator of transcription 6 activation and reduces lung inflammation in murine asthma, J. Allergy Clin. Immunol. 124 (2009) 607–610, https://doi.org/10.1016/j.jaci.2009.06.023, 610-611.
[30] S. Goenka, M.H. Kaplan, Transcriptional regulation by STAT6, Immunol. Res. 50 (2011) 87–96, https://doi.org/10.1007/s12026-011-8205-2.
[31] B.T. Kile, B.A. Schulman, W.S. Alexander, et al., The SOCS box: a tale of destruction and degradation, Trends Biochem. Sci. 27 (2002) 235–241, https://doi.org/10.1016/s0968-0004(02)02085-6.
[32] N. Liau, A. Laktyushin, I.S. Lucet, et al., The molecular basis of JAK/STAT inhibition by SOCS1, Nat. Commun. 9 (2018) 1558, https://doi.org/10.1038/s41467-018-04013-1.
[33] S.E. Wenzel, Y.Y. Tyurina, J. Zhao, et al., PEBP1 wardens ferroptosis by enabling lipoxygenase generation of lipid death signals, Cell 171 (2017) 628–641, https://doi.org/10.1016/j.cell.2017.09.044.
[34] J. Song, H. Zhang, Y. Tong, et al., Molecular mechanism of interleukin-17A regulating airway epithelial cell ferroptosis based on allergic asthma airway inflammation, Redox Biol. 68 (2023) 102970, https://doi.org/10.1016/j.redox.2023.102970.
[35] J. Zhao, H.H. Dar, Y. Deng, et al., PEBP1 acts as a rheostat between prosurvival autophagy and ferroptotic death in asthmatic epithelial cells, Proc. Natl. Acad. Sci. U.S.A. 117 (2020) 14376–14385, https://doi.org/10.1073/pnas.1921618117.
[36] J. Gao, J. Yuan, Q. Wang, et al., Metformin protects against PM(2.5)-induced lung injury and cardiac dysfunction independent of AMP-activated protein kinase alpha2, Redox Biol. 28 (2020) 101345, https://doi.org/10.1016/j.redox.2019.101345.
[37] D.R. Nagarkar, J.A. Poposki, M.R. Comeau, et al., Airway epithelial cells activate TH2 cytokine production in mast cells through IL-1 and thymic stromal lymphopoietin, J. Allergy Clin. Immunol. 130 (2012) 225–232, https://doi.org/10.1016/j.jaci.2012.04.019.
[38] C.S. Stevenson, M.A. Birrell, Moving towards a new generation of animal models for asthma and COPD with improved clinical relevance, Pharmacol. Ther. 130 (2011) 93–105, https://doi.org/10.1016/j.pharmthera.2010.10.008.
[39] M.E. Snitow, S. Li, M.P. Morley, et al., Ezh2 represses the basal cell lineage during lung endoderm development, Development 142 (2015) 108–117, https://doi.org/10.1242/dev.116947.
[40] R. Starr, T.A. Willson, E.M. Viney, et al., A family of cytokine-inducible inhibitors of signalling, Nature 387 (1997) 917–921, https://doi.org/10.1038/43206.
[41] W.W. Wang, K. Zhu, H.W. Yu, et al., Interleukin-17A potentiates interleukin-13-induced eotaxin-3 production by human nasal epithelial cells from patients with allergic rhinitis, Int. Forum Allergy Rhinol. 9 (2019) 1327–1333, https://doi.org/10.1002/alr.22382.
[42] V. Gielen, A. Sykes, J. Zhu, et al., Increased nuclear suppressor of cytokine signaling 1 in asthmatic bronchial epithelium suppresses rhinovirus induction of innate interferons, J. Allergy Clin. Immunol. 136 (2015) 177–188, https://doi.org/10.1016/j.jaci.2014.11.039.
[43] M. Federici, M.L. Giustizieri, C. Scarponi, et al., Impaired IFN-gamma-dependent inflammatory responses in human keratinocytes overexpressing the suppressor of cytokine signaling 1, J. Immunol. 169 (2002) 434–442, https://doi.org/10.4049/jimmunol.169.1.434.
[44] E. Doran, D.F. Choy, A. Shikotra, et al., Reduced epithelial suppressor of cytokine signalling 1 in severe eosinophilic asthma, Eur. Respir. J. 48 (2016) 715–725, https://doi.org/10.1183/13993003.00400-2015.
[45] S. Fukuyama, T. Nakano, T. Matsumoto, et al., Pulmonary suppressor of cytokine signaling-1 induced by IL-13 regulates allergic asthma phenotype, Am. J. Respir. Crit. Care Med. 179 (2009) 992–998, https://doi.org/10.1164/rccm.200806-992OC.
[46] G. Liu, C. Wei, S. Yuan, et al., Wogonoside attenuates liver fibrosis by triggering hepatic stellate cell ferroptosis through SOCS1/P53/SLC7A11 pathway, Phytother Res. 36 (2022) 4230–4243, https://doi.org/10.1002/ptr.7558.
[47] F. He, P. Zhang, J. Liu, et al., ATF4 suppresses hepatocarcinogenesis by inducing SLC7A11 (xCT) to block stress-related ferroptosis, J. Hepatol. 79 (2023) 362–377, https://doi.org/10.1016/j.jhep.2023.03.016.
[48] X. Liu, Y. Ma, L. Luo, et al., Dihydroquercetin suppresses cigarette smoke induced ferroptosis in the pathogenesis of chronic obstructive pulmonary disease by activating Nrf2-mediated pathway, Phytomedicine 96 (2022) 153894, https://doi.org/10.1016/j.phymed.2021.153894.
[49] S. Maschalidi, P. Mehrotra, B.N. Keceli, et al., Targeting SLC7A11 improves efferocytosis by dendritic cells and wound healing in diabetes, Nature 606 (2022) 776–784, https://doi.org/10.1038/s41586-022-04754-6.
[50] Y. Wang, R. Wan, W. Peng, et al., Quercetin alleviates ferroptosis accompanied by reducing M1 macrophage polarization during neutrophilic airway inflammation, Eur. J. Pharmacol. 938 (2023) 175407, https://doi.org/10.1016/j.ejphar.2022.175407.
[51] E. Habib, K. Linher-Melville, H.X. Lin, et al., Expression of xCT and activity of system xc(-) are regulated by NRF2 in human breast cancer cells in response to oxidative stress, Redox Biol. 5 (2015) 33–42, https://doi.org/10.1016/j.redox.2015.03.003.
[52] Y. Xu, Y. Li, J. Li, et al., Ethyl carbamate triggers ferroptosis in liver through inhibiting GSH synthesis and suppressing Nrf2 activation, Redox Biol. 53 (2022) 102349, https://doi.org/10.1016/j.redox.2022.102349.
[53] L. Jiang, N. Kon, T. Li, et al., Ferroptosis as a p53-mediated activity during tumour suppression, Nature 520 (2015) 57–62, https://doi.org/10.1038/nature14344.
[54] W. Zhang, Y. Sun, L. Bai, et al., RBMS1 regulates lung cancer ferroptosis through translational control of SLC7A11, J. Clin. Invest. 131 (2021), https://doi.org/10.1172/JCI152067.
[55] L. Liu, J. He, G. Sun, et al., The N6-methyladenosine modification enhances ferroptosis resistance through inhibiting SLC7A11 mRNA deadenylation in hepatoblastoma, Clin. Transl. Med. 12 (2022) e778, https://doi.org/10.1002/ctm2.778.
[56] P. Yadav, P. Sharma, S. Sundaram, et al., SLC7A11/xCT is a target of miR-5096 and its restoration partially rescues miR-5096-mediated ferroptosis and anti-tumor effects in human breast cancer cells, Cancer Lett. 522 (2021) 211–224, https://doi.org/10.1016/j.canlet.2021.09.033.
[57] T. Liu, L. Jiang, O. Tavana, et al., The deubiquitylase OTUB1 mediates ferroptosis via stabilization of SLC7A11, Cancer Res. 79 (2019) 1913–1924, https://doi.org/10.1158/0008-5472.CAN-18-3037.
[58] Y. Zhang, J. Shi, X. Liu, et al., BAP1 links metabolic regulation of ferroptosis to tumour suppression, Nat. Cell Biol. 20 (2018) 1181–1192, https://doi.org/10.1038/s41556-018-0178-0.
[59] Q. Chen, W. Zheng, J. Guan, et al., SOCS2-enhanced ubiquitination of SLC7A11 promotes ferroptosis and radiosensitization in hepatocellular carcinoma, Cell Death Differ. 30 (2023) 137–151, https://doi.org/10.1038/s41418-022-01051-7.
[60] L. Chen, J. Huang, Y.X. Ji, et al., Tripartite motif 8 contributes to pathological cardiac hypertrophy through enhancing transforming growth factor beta-activated kinase 1-dependent signaling pathways, Hypertension 69 (2017) 249–258, https://doi.org/10.1161/HYPERTENSIONAHA.116.07741.
[61] S.Y. Chen, H.P. Zhang, J. Li, et al., Tripartite motif-containing 27 attenuates liver ischemia/reperfusion injury by suppressing transforming growth factor beta-activated kinase 1 (TAK1) by TAK1 binding protein 2/3 degradation, Hepatology 73 (2021) 738–758, https://doi.org/10.1002/hep.31295.
[62] D. Jardine, M. Antolovich, P.D. Prenzler, et al., Liquid chromatography-mass spectrometry (LC-MS) investigation of the thiobarbituric acid reactive substances (TBARS) reaction, J. Agric. Food Chem. 50 (2002) 1720–1724, https://doi.org/10.1021/jf011336a.